

# 1 Progress in investigating long-term trends in the mesosphere, 2 thermosphere and ionosphere

3  
4  
5 Jan Laštovička

6  
7 Institute of Atmospheric Physics, Czech Acad. Sci., 14100 Prague, Czech Republic  
8  
9

10 *Correspondence to:* Jan Laštovička (jla@ufa.cas.cz)  
11  
12

13 **Abstract.** This article reviews main progress in investigations of long-term trends in the mesosphere,  
14 thermosphere and ionosphere over the period 2018-2022. Overall this progress may be considered significant.  
15 The research was most active in the area of trends in the mesosphere and lower thermosphere (MLT).  
16 Contradictions on CO<sub>2</sub> concentration trends in the MLT region have been solved; in the mesosphere trends do  
17 not differ statistically from trends near surface. The results on temperature trends in the MLT region are  
18 generally consistent with older results but develop and detailed them further. Trends in temperatures might  
19 significantly vary with local time and height in the whole height range of 30-110 km. Observational data indicate  
20 different wind trends in the MLT region up to sign of trend in different geographic regions, which is supported  
21 by model simulations. Changes in semidiurnal tide were found to differ according to altitude and latitude. Water  
22 vapor concentration was found to be the main driver of positive trends in brightness and occurrence frequency of  
23 noctilucent clouds (NLC), whereas cooling through mesospheric shrinking is responsible for slight decrease in  
24 NLC heights. The research activity in the thermosphere was substantially lower. The negative trend of  
25 thermospheric density continues without any evidence of a clear dependence on solar activity, which results in  
26 an increasing concentration of dangerous space debris. Significant progress was reached in long-term trends in  
27 the E-region ionosphere, namely in foE (critical frequency of E-region corresponding to its maximum electron  
28 density). These trends were found to depend principally on local time up to their sign; this dependence is strong  
29 at European high midlatitudes but much less pronounced at European low midlatitudes. In the ionospheric F2-  
30 region very long data series (starting at 1947) of foF2 revealed very weak but statistically significant negative  
31 trends. First results on long-term trends were reported for the topside ionosphere electron densities (near 840  
32 km), the equatorial plasma bubbles and the polar mesospheric summer echoes. The most important driver of  
33 trends in the upper atmosphere is the increasing concentration of CO<sub>2</sub> but other drivers also play a role. The most  
34 studied one was the effect of the secular change of the Earth's magnetic field. The results of extensive modeling  
35 reveal the dominance of secular magnetic change in trends in foF2 (critical frequency corresponding to the  
36 maximum electron density in the ionosphere) and its height hmF2, total electron content and electron  
37 temperature in the sector of about 50°S-20°N and 60°W-20°E. However, its effect is locally both positive and  
38 negative, so in the global average this effect is negligible. The first global simulation with model WACCM-X of

39 changes of temperature excited by anthropogenic trace gases simultaneously from surface to the base of  
40 exosphere provides results generally consistent with observational pattern of trends. Simulation of ionospheric  
41 trends over the whole Holocene (9455 BC – 2015) was reported for the first time. Various problems of long-term  
42 trend calculations are also discussed. There are still various challenges in further development of our  
43 understanding of long-term trends in the upper atmosphere. The key problem is the long-term trends in  
44 dynamics, particularly in activity of atmospheric waves, which affect all layers of the upper atmosphere. At  
45 present we only know that these trends might be regionally different, even opposite.

46  
47

## 48 **1 Introduction**

49

50 The anthropogenic emissions of polluting substances, greenhouse gases and ozone depleting substances  
51 (ODS), also affect the upper atmosphere, including the mesosphere (~50–90 km), the thermosphere (~90–1000  
52 km), and the ionosphere, which is embedded in the upper atmosphere (e.g., Rishbeth and Roble 1992; Laštovička  
53 et al., 2006). The thermosphere is the operating environment of many satellites, including the International Space  
54 Station, and thousands of pieces of space debris, the orbital lifetime of which depends on long-term changes of  
55 thermospheric density. Propagation of Global Positioning System (GPS) signals and radio communications are  
56 affected by the ionosphere, thus anthropogenic changes of these high-altitude regions can affect also satellite-  
57 based technologies which are increasingly important to modern life. The challenge facing upper atmosphere  
58 climate scientists is to detect long-term trends and understand their primary causes, so that society can mitigate  
59 potential harmful changes.

60 Greenhouse gases in the troposphere are optically thick to outgoing longwave (infrared) radiation, which they  
61 both absorb and reemit back to the surface to produce the heating effect. In contrast, greenhouse gases, mainly  
62 CO<sub>2</sub> in the much lower density upper atmosphere are optically thin to outgoing infrared radiation and the other  
63 property of CO<sub>2</sub>, strong infrared emission, dominates. In-situ collisional excitation results in atmospheric thermal  
64 energy readily lost to space via outgoing infrared radiation, while the absorption of radiation emanating from the  
65 lower atmosphere plays only a secondary role in the energy balance. The net result is that the radiatively active  
66 greenhouse gases act as cooling agents, and their increasing concentrations enhance the cooling effect in the  
67 upper atmosphere. This effect of greenhouse gases may be called “greenhouse cooling” (Cicerone 1990).

68 The cooling results in thermal contraction of the upper atmosphere and related significant decline in  
69 thermospheric density at fixed heights, which was observed in long-term satellite drag data (e.g., Emmert et al.  
70 2008). Downward displacement of ionospheric layers should accompany this contraction. The cooling also  
71 affects chemical reaction rates and, thus, the chemistry of minor constituents, resulting in further changes to the  
72 ionosphere.

73 Investigations of long-term changes in the upper atmosphere and ionosphere began with the pioneering study  
74 of Roble and Dickinson (1989). They suggested that global cooling will occur in the upper atmosphere due to the  
75 long-term increase of greenhouse gas concentrations, particularly carbon dioxide (CO<sub>2</sub>). Modeling studies by  
76 Rishbeth (1990) and Rishbeth and Roble (1992) broadened these results to the thermosphere-ionosphere system.  
77 First observational studies of long-term trends in the ionosphere were those by Aikin et al. (1991) and by  
78 Laštovička and Pancheva (1991).

79 With the increasing amount of observational and model results and findings, a global pattern of trend  
80 behavior began to emerge, and, in 2006, the first global scenario of trends in the upper atmosphere and  
81 ionosphere was constructed (Laštovička et al., 2006a, 2008a). Since 2006 other parameters were added to this  
82 scenario, some discrepancies were removed and/or explained, and in recent years it became increasingly clear  
83 that non-CO<sub>2</sub> drivers also play an important role in long-term trends in the upper atmosphere and ionosphere  
84 together with the dominant increasing atmospheric concentration of greenhouse gases, mainly of CO<sub>2</sub>.

85 Various papers summarizing and discussing long-term trends and various aspects of their investigations have  
86 been published in recent years. Laštovička (2017) summarized progress in investigating long-term trends in the  
87 mesosphere, thermosphere and ionosphere in the period 2013-2016. Laštovička and Jelínek (2019) summarized  
88 and discussed problems associated with calculating long-term trends in the upper atmosphere (see section 2).

89 Danilov and Konstantinova (2020a) reviewed long-term variations in the middle and upper atmosphere and in  
90 the ionosphere. The middle atmosphere (stratosphere, mesosphere and mesopause region) cooling trend has  
91 reliably been established from observations by different methods. On the other hand, there are noticeable  
92 discrepancies in estimates of negative trends in the critical frequency foF2, which corresponds to the maximum  
93 ionospheric electron density, and in its height hmF2. Processes in the mesosphere and thermosphere have been  
94 more rapid than predicted by models.

95 Elias et al. (2022) reviewed long-term trends in the equatorial ionosphere due to the secular variation of the  
96 Earth's magnetic field. This effect occurs in the F2 layer of the ionosphere; in lower levels below the F2 layer it  
97 is negligible. Low and equatorial latitudes are more sensitive to the secular change of the Earth's magnetic field  
98 than middle latitudes.

99 Laštovička (2022) reviewed trends in foF2 from the point of view of space climate. These trends are  
100 relatively weak. Different methods of trend determination and of reduction of effect of solar cycle result in  
101 differences in trends in foF2.

102 Danilov and Berbenova (2021) reviewed applied aspects of long-term trends in the upper atmosphere.  
103 Increasing H<sub>2</sub>O concentration in the middle atmosphere can affect the state of ozone layer and also polar  
104 mesospheric summer echoes (PMSE). Modifications of systems of winds and intensification of upward  
105 penetration of gravity waves into the ionosphere could result in intensification of "meteorological control" of  
106 ionosphere. Thermospheric cooling and related decrease of thermospheric density at satellite altitudes prolong  
107 orbital lifetime of space debris and thus increase the probability of dangerous collisions of space vehicles with  
108 space debris. Trends of the total electron content (in unit column, TEC) and ionospheric slab thickness (the ratio  
109 of TEC to the F2-layer peak electron density) are related to corrections of positioning systems. Trends in foF2  
110 affect propagation of short radio waves.

111 Here I report progress in the long-term trend investigations in the mesosphere, thermosphere and ionosphere  
112 over the period 2018-2022. Section 2 describes problems in calculating long-term trends. Section 3 examines  
113 trends in the mesosphere and lower thermosphere. Section 4 describes progress in studying thermospheric trends.  
114 Section 5 examines long-term trends in the ionosphere. Section 6 describes progress in global or very-long-term  
115 modeling. Section 7 examines roles of non-CO<sub>2</sub> drivers of trends. Section 8 contains conclusions.

## 116 117 118 **2 Problems in Calculating Long-Term Trends**

119

120 Laštovička and Jelínek (2019) summarized and discussed problems associated with calculating long-term  
121 trends in the upper atmosphere. Calculations of long-term trends in the upper atmosphere suffer with various  
122 problems, which may be divided into three groups: (1) natural variability, (2) data problems, and (3)  
123 methodology. These problems have often been underestimated in trend calculations in the past, which led to  
124 controversial trend results. In the upper atmosphere there is a strong influence of the 11-year solar cycle, which  
125 has to be removed as much as possible. Different solar activity proxies used may result in clearly different  
126 trends, particularly for foF2 (e.g., Laštovička, 2021b), as it is illustrated by Fig. 1. There are also other trend  
127 drivers (see section 7), which modify the CO<sub>2</sub>-driven trend. A serious problem of trend investigations is  
128 homogeneity of long-term data series, which should be carefully checked before beginning trend calculations.  
129 The simplest method of trend calculation is the linear regression method, which is however often  
130 oversimplification. Then the multiple linear regression or piecewise linear regression can be applied, or more  
131 sophisticated methods like artificial neural networks, machine learning, or the ensemble empirical mode  
132 decomposition. Assumption of methods and their sensitivity to error propagation (effects of errors in data)  
133 should be considered. The selection of suitable method should be data driven. It should also be noted that trends  
134 calculated in terms of fixed heights versus fixed pressure levels might be different, sometimes even substantially.

135

136 **Figure 1.**

137

138 The problem of the most suitable solar activity proxy for ionospheric investigations was treated by Laštovička  
139 (2019, 2021a, 2021b). They used yearly average and monthly median foF2 data of three midlatitude European  
140 stations, Juliusruh (54.6°N, 13.4°E), Pruhonice (50.0°N, 14.6°E) and Rome (41.8°N, 12.5°E) and six solar  
141 activity proxies, F10.7, F30, Mg II, He II, sunspot numbers and the solar H Lyman- $\alpha$  flux, analyzed over two  
142 periods, 1976-1995 and 1996-2014. This analysis suggests F30 and Mg II as the most suitable solar activity  
143 proxies, not the traditionally used proxies F10.7 and sunspot numbers. Preliminary results for yearly foE (critical  
144 frequency of ionospheric E-region, corresponding to its electron density maximum), based on data of stations  
145 Juliusruh and Slough/Chilton (51.7°N, 1.3°W), favor rather F10.7. Danilov (2021) reported that the relationship  
146 between F10.7 and three other solar activity proxies, sunspot number, Mg II and Lyman- $\alpha$  flux, is close in solar  
147 cycles 22 and 23 but differs in cycle 24, for which he suggested correction of F10.7 for foF2 long-term  
148 investigations.

149 Danilov and Konstantinova (2020b) estimated foF2 trends of stations Juliusruh and Boulder (40.0°N,  
150 105.0°W) until 2018 and found peculiar foF2 trend changes in solar cycle 24. To get reasonable foF2 trend  
151 compared to previous period, F10.7 has to be corrected with sunspot number and the solar Lyman alpha flux  
152 values. Danilov and Konstantinova (2020c) found the same problem and the same solution for hmF2.

153 Huang et al. (2020) claim that due to the seasonal dependence of the relationship between NmF2 (the  
154 maximum electron density in the ionosphere located at the maximum of F2 region) and solar EUV (extreme  
155 ultraviolet) irradiance the application of yearly values (average from monthly average values) to trend  
156 calculations may result both in positive or negative biases. For Juliusruh, 1970-2014, they obtained trends  
157  $0.0089 \pm 0.0044 \times 10^{11} \text{ el m}^{-3} \text{ year}^{-1}$  for yearly average values,  $0.0100 \pm 0.0033 \times 10^{11}$  for monthly average values,

158 and  $0.0091 \pm 0.0033 \times 10^{11}$  for bias-corrected yearly values. However, all differences between the above trends  
159 are within error bars, i.e. they are not statistically significant.

160 It should be mentioned here that an important problem of some trend calculations may be atmospheric tides.  
161 The impact of atmospheric tides via data sampling might be important when the local time of measurement is not  
162 fixed or where there are trends in the tides that make the trend dependent on the local time. One more problem is  
163 that particularly ionospheric trends might be strongly seasonally and diurnally (local time) dependent up to the  
164 change of trend sign as it is demonstrated in section 5; this is not the effect of tides.

165

## 166 **2.1 Summary**

167

168 Main progress was made in shedding light on problems related to natural variability, mainly on the critical  
169 problem of removal/suppression of the effect of the solar cycle using various solar activity proxies, and also in  
170 specifying problems of solar cycle 24. As concerns data problems, i.e. mainly homogeneity of long data series,  
171 there are various techniques how to detect discontinuities and other possible problems, which are used among  
172 others in climatology and meteorology, so no special techniques are needed to be developed for the upper  
173 atmosphere. As concerns methodology, we may use methods developed for climatological and meteorological  
174 investigations and other available techniques but as data show, often it is sufficient to use simple or multi-  
175 parameter regression, because the long-term trend signals and signal-to-noise ratios are often substantially  
176 stronger than in the troposphere. On the other hand, the amount of data available in the upper atmosphere is  
177 much smaller and data series shorter than those in the troposphere.

178

179

## 180 **3 Mesosphere and Lower Thermosphere**

181

182 Long-term trends in various parameters have been investigated in the mesosphere and lower thermosphere  
183 (altitudes about 50-120 km, MLT region). The most studied parameter has been temperature but both zonal and  
184 meridional winds, minor constituents, noctilucent clouds, water vapor concentration and some other parameters  
185 have been studied as well. We begin review with observational results on trends in temperature. Many of such  
186 studies were based on SABER (Sounding of the Atmosphere using Broadband Emission Radiometry)  
187 observations onboard satellite TIMED (Thermosphere Ionosphere Mesosphere Energetics and Dynamics).

188 The 17 years (2000-2016) long midnight spectral OH\* airglow measurements at Zvenigorod (56°N, 37°E)  
189 revealed a weak negative trend of mesopause region temperature of  $-0.7 \pm 0.3$  K/decade (Perminov et al., 2018).

190 Continuous Na lidar measurements of nocturnal mesopause region characteristics at Fort Collins (41°N,  
191 105°W) and Logan (42°N, 112°W) over 1990-2018 revealed a cooling trend larger than  $-2$  K/decade and a  
192 decrease of the wintertime upper mesopause height (above 97 km) by  $-450$  m/decade and of the lower non-  
193 winter mesopause (height below 92 km) by  $-130$  m/decade. The WACCM-X (Whole Atmosphere Community  
194 Climate Model eXtended) model provides similar changes of the mesopause heights caused mainly by cooling  
195 and contraction of the stratosphere and lower mesosphere (Yuan et al., 2019).

196 She et al. (2019) reported results of nighttime temperature measurements by a midlatitude Na lidar over 1990-  
197 2017. The height profile of the 28-year long temperature data trend begins with a weak positive warming at 85

198 km, continues with cooling at 87(88) km with maximal cooling at 92(93) km, and it turns to a warming trend at  
199 102(100) km. Wintertime trend is much cooler than summertime trend. The lidar temperature trends generally  
200 agree with SABER temperatures and within error bars also with model LIMA (Leibniz-Institute Middle  
201 Atmosphere Model). They also show that data sets longer than two solar cycles are necessary to obtain reliable  
202 long-term trend.

203 Li et al. (2021) merged middle atmosphere temperature observations from HALOE (Halogen Occultation  
204 Experiment, 1991-2005) and SABER (2002-2019) in 45°S-45°N. They found stronger mesospheric cooling at  
205 the Southern Hemisphere (SH) than at the Northern Hemisphere (NH), which peaks at 60-70 km with trend of -  
206 1.2 K/decade. The temperature trend derived from SABER data only is by a factor of 1.5 weaker than that based  
207 on merged data, which is consistent with some upper stratosphere ozone recovery after the mid-1990s.

208 Venkat Ratnam et al. (2019) merged data on the middle atmosphere over India obtained by various measuring  
209 techniques (rockets, High-Resolution Doppler Imager (HRDI)/ Upper Atmosphere Research Satellite (UARS),  
210 (HALOE)/UARS, SABER/TIMED and Mesosphere-Stratosphere-Troposphere (MST) radars) across more than  
211 25 years. The observational analysis was accompanied by WACCM-X model simulations. They found  
212 significant cooling trend  $-1.7 \pm 0.5$  K/decade between 30 and 80 km heights. All observed changes are well  
213 captured by the WACCM-X simulations if changes in greenhouse gas concentrations are included.

214 24 years of measurements of OH nightglow rotational temperature at Davis, Antarctica (68°S, 78°E) revealed  
215 a cooling trend of  $-1.2 \pm 0.51$  K/decade (French et al., 2020). The comparison for the last 14 years of trend with  
216 trend derived from Aura/MLS (Microwave Limb Sounder) at a level of 0.00464 hPa gives very good agreement.

217 Dalin et al. (2020) reported update of long-term trends of mesopause temperature in Moscow region (around  
218 55°N). They observed statistically cooling of the summer mesopause region by  $-2.4 \pm 2.3$  K/decade and an  
219 insignificant and small cooling in winter for the period 2000-2018.

220 Huang and Mayr (2021) analyzed zonal mean SABER temperatures over 2002-2014. They found that trends  
221 might significantly vary with local time and height in the whole height range of 30-110 km. Figure 2 shows that  
222 even for zonal mean temperatures the trends at 00:00, 06:00, 12:00 and 18:00 LT (local time) differ evidently,  
223 particularly for 12:00 and 18:00 LT and above about 75 km. However, it is possible that with a longer data series  
224 available the differences would be smaller.

225

## 226 **Figure 2**

227

228 Bailey et al. (2021) created temporal series of mesospheric temperatures and pressure altitudes by combining  
229 observations from HALOE, SABER and SOFIE (Solar Occultation for Ice Experiment) for June at the Northern  
230 Hemisphere (NH) and December at the Southern Hemisphere (SH) for latitudes 64°-70°. They found a robust  
231 result that the mesosphere generally cools at most heights by 1-2 K/decade in response to the increasing  
232 greenhouse gas concentrations, the cooling peaking near 0.03 hPa at NH and 0.05 hPa at SH. This cooling results  
233 in atmospheric shrinking by 100-200 m/decade. Shrinking results in reduced cooling and eventually heating near  
234 0.005 hPa due to hydrostatic contraction.

235 Zhao et al. (2020) examined global distribution and changes of monthly average mesopause temperatures  
236 based on SABER measurements at latitudes 83°S-83°N over 2002-2019. They observed cooling at all latitudes  
237 ranging from ~0 to -1.4 K/decade with a mean value  $-0.75 \pm 0.43$  K/decade with stronger cooling on SH than on

238 NH. At high latitudes, the cooling is significant in non-summer season; there is no significant trend in summer.  
239 They observed the weakest trends in 40°-60°N and the strongest trends in 60°-80°S.

240 Das (2021) examined SABER temperature data for long-term trends over 2003-2019 using the empirical  
241 mode decomposition method. He confirmed global cooling of the middle atmosphere and found long-term trends  
242 of -0.5 K/decade in the lower mesosphere and -1.0 K/decade in the upper mesosphere. The SH mesopause and  
243 NH stratopause exhibit stronger cooling than the opposite hemisphere. The SH mesopause shows stronger  
244 cooling over Indian Ocean.

245 Zhao et al. (2021) presented another analysis of SABER temperature measurements for 2002-2020 at heights  
246 of 20-110 km. The near-global mean temperature exhibits consistent cooling trends throughout the middle  
247 atmosphere ranging from -0.28 up to -0.97 K/decade.

248 Bizuneh et al. (2022) analyzed long-term mesospheric (60-100 km) variability of temperature and ozone  
249 mixing ratio as measured by SABER over 2005-2020 at latitudes 5°-15°N. They found negative trends in  
250 temperature and ozone in the lower mesosphere of -0.85 K/decade and -0.12 ppmv/decade, respectively, and  
251 positive trends in 85-100 km of 1.25 K/decade and 0.27 ppmv/decade, respectively. Both temperature and ozone  
252 are affected by F10.7, El Niño–Southern Oscillation (ENSO, Niño 3.4 index) and the Quasi-Biennial Oscillation  
253 (QBO, QBO<sub>30</sub> index).

254 Mlynczak et al. (2022) used SABER/TIMED observations over 2002-2021 to study the behavior of the MLT  
255 region. They found significant cooling and contraction from 2002 to 2019 (solar cycle minimum) due to weaker  
256 solar cycle and increasing CO<sub>2</sub>. The MLT thickness between 1 and 10<sup>-4</sup> hPa contracted by 1333 m, out of which  
257 342 m can be attributed to increasing CO<sub>2</sub>. The MLT region sensitivity to CO<sub>2</sub> doubling was estimated to be -  
258 7.5 K according to the observed temperature trends and CO<sub>2</sub> growth rate.

259 Rayleigh lidar observations at Observatoire de Haute Provence (44°N, 6°E), which cover four decades, did  
260 not reveal any long-term change of mesospheric temperature inversion layers potentially related to climate  
261 change (Ardalan et al., 2022). Only an interannual variability with quasi decadal oscillations was observed.

262 The observational analyses have been accompanied and supported by model simulation analyses of long-term  
263 trends in the MLT region temperatures, which are reported below.

264 Qian et al. (2019) simulated trends in mesospheric temperature and winds with model WACCM-X and  
265 compared them with winds observed at Collm over 1980-2014. They found a global temperature trend in the  
266 mesosphere to be negative in line with observations, and reaching a maximum of about -1 K/decade in the  
267 middle and lower mesosphere (~55-65 km). The temperature trend becomes near zero or even slightly positive in  
268 the summer upper mesosphere. This is likely due to dynamical effects associated with the mesospheric  
269 meridional circulation that is driven by the breaking of upward propagating gravity waves (Qian et al., 2019).

270 Kuilman et al. (2020) simulated the impact of CO<sub>2</sub> doubling on the middle atmosphere with model WACCM;  
271 they found the direct mesospheric cooling to reach up to 15 K.

272 Ramesh et al. (2020b) simulated long-term (1850-2014) variability of temperature and zonal wind with model  
273 WACCM-6. They confirmed CO<sub>2</sub> and ozone depleting substances (ODS) to be the main drivers of the observed  
274 cooling of the middle atmosphere. The simulated cooling was stronger in the lower mesosphere than at higher  
275 mesospheric levels.

276 Another important parameter is wind. Trends in winds, particularly in zonal wind, were studied both with  
277 observations and model simulations.

278 Venkat Ratnam et al. (2019) carefully merged data on the middle atmosphere (stratosphere, mesosphere and  
279 lower thermosphere) over India obtained by various measuring techniques (rockets, HRDI/UARS,  
280 HALOE/UARS, SABER/TIMED and MT radars) over more than 25 years. The eastward zonal wind trend was  
281 large, about  $-5 \text{ ms}^{-1}/\text{decade}$ , but statistically significant only in 70-80 km, which resulted in change from a strong  
282 eastward in the 1970s to a weak westward in the last decade; no significant trend was found in meridional wind.  
283 All observed changes are well captured by the WACCM-X simulations if changes in greenhouse gas  
284 concentrations are included.

285 Meteor radar winds measured at Andenes (69.3°N, 16°E), Juliusruh (54.6°N, 13.4°E) and Tavistock (43.3°N,  
286 80.8°W) over 2002-2018 revealed annual wind tendency toward south and west (up to  $3 \text{ ms}^{-1}/\text{decade}$ ) for  
287 Andenes but slight opposite to negligible tendencies at midlatitudes (Wilhelm et al., 2019).

288 Vincent et al. (2019) derived vertical wind velocities from the divergence of mean meridional wind measured  
289 by MF (medium frequency) radar above Davis, Antarctica (69°S, 78°E) over 1994-2018 in the three weeks just  
290 after summer solstice. The estimated vertical velocity peak values varied between 2 and 6 cm/s with significant  
291 interannual variability. These peak values did not exhibit a significant long-term change but the height of wind  
292 maximum displayed a statistically significant long-term decrease of about  $-0.6 \text{ km}/\text{decade}$ .

293 Qian et al. (2019) simulated with model WACCM-X trends in mesospheric temperature and winds and  
294 compared them with winds observed at Collm over 1980-2014. They found as Figure 3 shows that trends in  
295 winds near an altitude of 90 km reveal a dynamical pattern with regionally both positive and negative values  
296 within about  $\pm 5 \text{ ms}^{-1}/\text{decade}$ , which indicates predominant control by dynamics. Figure 3 illustrates how  
297 complex are trends in winds and how difficult is to investigate them.

298

299 **Figure 3.**

300

301 Kogure et al. (2022) focused on mechanisms of the thermospheric zonal mean wind response to doubling the  
302  $\text{CO}_2$  concentration based on model GAIA (Ground-to-topside model of Atmosphere and Ionosphere for  
303 Aeronomy) simulations. The pattern is very complex; three main forces, ion drag, molecular viscosity and  
304 meridional pressure gradient, strongly attenuate each other.

305 Atmospheric waves, namely gravity waves, planetary waves and tides, are a very important vertical coupling  
306 mechanism between the upper atmosphere and ionosphere, and the lower atmosphere below. Unfortunately there  
307 was little activity in investigating trends in wave activity.

308 Meteor radar winds measured at Andenes (69.3°N, 16°E), Juliusruh (54.6°N, 13.4°E) and Tavistock (43.3°N,  
309 80.8°W) over 2002-2018 revealed no significant trend in diurnal tides and changes of semidiurnal tide, which  
310 differ according to altitude and latitude (Wilhelm et al., 2019).

311 The WACCM6 model simulated trends of the diurnal migrating tide amplitude in the MLT region (0.0001-  
312 0.01 hPa) for the period 1850-2014. Trends were found to be positive, mainly due to the increasing concentration  
313 of  $\text{CO}_2$  with some contribution of trend of ENSO (Ramesh et al., 2020a).

314 Ramesh and Smith (2021) used WACCM6 simulations over 1850-2014 and found the increasing non-  
315 migrating diurnal tide in the MLT region (0.0001-0.01 hPa) in temperature, zonal and meridional winds,  
316 particularly at low and equatorial latitudes, predominantly due to the increasing concentration of  $\text{CO}_2$ .



317 New results were obtained in studies of long-term trends in the MLT region composition, namely in CO<sub>2</sub> and  
318 water vapor, and related trends in noctilucent clouds, called also polar mesospheric clouds when they are  
319 observed from above by satellites.

320 Rezac et al. (2018) analyzed long-term trends of CO<sub>2</sub> based on direct SABER measurements. They found that  
321 below 90 km the CO<sub>2</sub> trends statistically do not differ from the surface/tropospheric CO<sub>2</sub> trends in agreement  
322 with model simulations, whereas above 90 km up to 110 km (top height of measurements) the CO<sub>2</sub> trends are  
323 slightly higher but less than provided by previous analyses. This important study closed several years of  
324 discussions of satellite-based trend of CO<sub>2</sub>, which was originally reported to be higher than near surface.

325 Yu et al. (2022) studied water vapor evolution in the tropical middle atmosphere with the merged dataset of  
326 satellite observations between 1993 and 2020 and model SD-WACCM (WACCM6 with specified dynamics)  
327 simulations over 1980-2020. They found a relatively weak trend 0.1 ppmv/decade in observations and no trend  
328 in simulations. Simulations revealed periods of increasing as well as decreasing mesospheric water vapor due to  
329 non-linear changes of methane emissions and sometimes irregular changes in the tropical tropopause  
330 temperature.

331 Nedoluha et al. (2022) examined measurements of mesospheric water vapor by the Water Vapor Millimeter-  
332 wave Spectrometers (WVMS) at three stations in California, Hawaii and New Zealand from 1992 to 2021 and  
333 compared them with measurements onboard satellites by HALOE, SABER and Aura/MLS. Differences between  
334 ground-based and satellite trends vary within ~3 %/decade. This uncertainty is comparable with trends of  
335 mesospheric water vapor since the early 1990s. The increase of CH<sub>4</sub> concentration over the last 30 years should  
336 increase H<sub>2</sub>O mixing ratio by ~4%, which corresponds to trend 1.3 %/decade. Such a trend is within the range of  
337 trends and their uncertainties derived from measurements of other WVMS instruments.

338 Yue et al. (2019) report an increase of water vapor concentration in the mesosphere over 2002-2018 by 0.1-  
339 0.2 ppmv/decade according to SABER measurements and 0.2-0.3 ppmv/decade according to Aura/MLS  
340 measurements. The trend is somewhat stronger in the lower and upper mesosphere. WACCM simulations  
341 provide the same trend of water vapor as observations in the lower mesosphere. The origin of water vapor trend  
342 is partially dissociation of methane (mainly above 65 km), and partially transport of water vapor from below.

343 On the other hand, measurements of the mesospheric water vapor concentration by the radiometer  
344 MIAWARA (Middle Atmospheric WATER vapor RADIometer) in Zimmerwald (46.88°N, 7.46°E) in Switzerland  
345 over 2007-2018 displayed significant decrease of water vapor concentration with a rate of  $-0.60 \pm 0.02$   
346 ppmv/decade at heights of 61-72 km (Lainer et al., 2019). Authors were not able to give an explanation for the  
347 origin of the detected water vapor decline.

348 A 138-years long model simulation of the impact of increasing concentration of CO<sub>2</sub> and methane near 83 km  
349 altitude revealed a substantial increase of the noctilucent cloud (NLC) brightness due to ~40% increase of water  
350 vapor induced by increasing methane concentration (Lübken et al., 2018). This increase is qualitatively  
351 consistent with polar mesospheric cloud observations by satellites. The origin of water vapor trend is partially  
352 dissociation of methane (mainly above 65 km), and partially transport of water vapor from below.

353 Lübken et al. (2021) analyzed long-term trends in mesospheric ice layers derived from simulations with  
354 models LIMA and MIMAS (Mesospheric Ice Microphysics And tranSPort model) over the period of 1871-2008  
355 for middle (58°N), high (69°N) and Arctic (78°N) latitudes. Increases of ice particle radii and NLC brightness

356 with time are mainly caused by an enhancement of water vapor. The negative trend of NLC heights is primarily  
357 caused by CO<sub>2</sub>-induced cooling at lower heights.

358 Dalin et al. (2020) reported an update of long-term trends in noctilucent clouds in Moscow region around  
359 55°N. Trends in noctilucent clouds over 1968-2018 were small and insignificant in agreement with other  
360 observations from comparable latitudes.

361 Long-term trends have been studied also in other parameters of the mesosphere and lower thermosphere, in  
362 airglow, polar mesospheric summer echoes, or summer length (defined using spring and autumn wind reversal)  
363 in the MLT region.

364 Huang (2018) used the 55-year long series of results of simulations by two models focused on examining the  
365 effect of increasing CO<sub>2</sub> concentration on airglow intensity, volume emission ratio (VER) and VER peak height.  
366 He found weak and opposite linear trends of airglow intensities of OH(8,3), O(0,1) and O(<sup>1</sup>S) spectral lines and  
367 of VER with increasing CO<sub>2</sub>, whereas the VER peak height strongly and out-of-phase correlated with  
368 geomagnetic activity.

369 Observations of mesopause airglow emissions of O<sub>2</sub>(A 0-1) and OH (6-2) at Zvenigorod (55.4°N, 36.5°E)  
370 over 2000-2019 provided a trend of average yearly emissions of -33±3 and -26±0.2 %/decade, respectively  
371 (Perminov et al., 2021), which is surprisingly strong trend.

372 Dalin et al. (2020) reported update of long-term trends in airglow emission intensity in Moscow region. They  
373 found statistically significant negative trends in the intensities of O<sub>2</sub> A(0-1) and OH (6-2) airglows both in  
374 summer and winter for the period 2000-2018.

375 Based on radar observations at Andoya (69.5°N, 16.7°E) over 1994-2020, Latteck et al. (2021) obtained after  
376 eliminating the effects of solar and geomagnetic activity a polar mesospheric summer echo trend of  
377 3.2%/decade, which might be related to the observed negative trend of mesospheric temperatures in polar  
378 latitudes.

379 Mesospheric wind measurements by specular meteor radars and partial reflection radars over northern  
380 Germany (~54°N) and northern Norway (~69°N) between 2004-2020 using two definitions of summer length  
381 provided a positive trend of summer length for the mesosphere only but no clear trend for the whole MLT  
382 region. 31 year midlatitude partial reflection radar data indicate break point and non-uniform trend of summer  
383 length, i.e. 1990-2008 a slight negative trend, break in 2008, and a positive trend in 2008-2020 (Jaen et al.,  
384 2022).

385 Simulations with NASA (National Atmospheric and Space Administration) model E2.2-AP reveal impact of  
386 CO<sub>2</sub> on the quasi-biennial oscillation (QBO). The increasing concentration of CO<sub>2</sub> results in reduction of the  
387 QBO period (Dalla Santa et al., 2021). QBO is a stratospheric phenomenon but with impact on the mesosphere.

388

### 389 **3.1 Summary**

390

391 The mesosphere and lower thermosphere was the most actively studied region of the upper atmosphere and  
392 ionosphere system in the past five years from the point of view of long-term trends. The most studied parameter  
393 was temperature both due to its importance (the primary direct effect of increasing concentration of CO<sub>2</sub> at  
394 heights above ~50 km is radiative cooling) and availability of both ground-based and satellite-based data as well  
395 as of model simulations. The general pattern is cooling, particularly in the mesosphere, but various observations

396 are only mostly but not fully consistent, partially maybe due to insufficient length of data series used; She et al.  
397 (2019) claim that data sets longer than two solar cycles are necessary to obtain reliable long-term trend. Huang  
398 and Mayr (2021) found that trends might significantly vary with local time and height in the whole height range  
399 of 30-110 km but they studied data series only 13 years long. Also model simulations provide general cooling,  
400 even though the WACCM simulations by Qian et al. (2019) indicate that the temperature trend becomes near  
401 zero or even slightly positive in the summer upper mesosphere, likely due to dynamic effects (winds and  
402 atmospheric wave activity). The results on temperature trends are generally consistent with older results. It  
403 should be mentioned that temperature trends are affected also by the stratospheric ozone behavior, which was  
404 highly non-linear due to change after the mid-1990s from relatively rapid decline to much weaker decline,  
405 stagnation or recovery (depending on region and altitude). In summary, it is clear that long-term trends in the  
406 MLT temperature are now better known and understood than before 2018; our knowledge broadened and it is  
407 more detailed; e.g. trends are now better quantified, model-derived trends are in agreement with observational  
408 trends, and some hemispheric asymmetry of temperature trends was found.

409 Dynamical parameters, such as winds and atmospheric waves, play a critical role in the MLT region. Here  
410 the trend pattern is much more complex. Observational data indicate different wind trends up to sign of trend in  
411 different geographic regions (e.g., Wilhelm et al., 2019). Simulations (Qian et al., 2019) show that trends in  
412 winds reveal a dynamical pattern with both positive and negative values. A limited activity in the area of  
413 atmospheric waves was focused on tides in 2018-2022. Meteor radar wind data from high/middle latitudes  
414 revealed no significant trend in diurnal tides and changes of semidiurnal tide, which differ according to altitude  
415 and latitude (Wilhelm et al., 2019). On the other hand simulations with WACCM6 provide positive trends for  
416 both migrating and non-migrating diurnal tides. Trends in dynamical parameters are not well understood, which  
417 is the key problem of trend studies in the upper atmosphere. They seem to be substantially regionally dependent.

418 Another group of parameters are CO<sub>2</sub>, water vapor and noctilucent clouds. Rezac et al. (2018) finally solved  
419 contradictions about evaluations of satellite measurements of concentration of CO<sub>2</sub>, which is the result of  
420 principal importance. It was found that the CO<sub>2</sub> concentration trends in the mesosphere (below 90 km) do not  
421 differ statistically from trends at surface, even though they appear to be slightly larger above 90 km. Water vapor  
422 trends in the mesosphere are generally positive; it is only in the equatorial region that trends are very little or  
423 near-zero. The only exception is radiometer measurements in Switzerland with significant negative trend at  
424 heights 61-72 km with an unknown explanation. As for noctilucent clouds, recent results confirm positive  
425 trends, which weaken with decreasing latitude. This trend is mainly due to the increase of water vapor  
426 concentration. Their height is slightly decreasing primarily due to mesospheric shrinking due to CO<sub>2</sub>-induced  
427 cooling at lower heights.

428 Long-term trends were studied also in other parameters. Airglow intensities in different spectral lines have  
429 different and even opposite trends, even though negative trends dominate. Polar mesospheric summer echo trend  
430 was found to be positive, which might be related to the observed negative trend of mesospheric temperatures in  
431 polar latitudes. Midlatitude partial reflection radar data indicate break point and non-uniform trend of  
432 mesospheric summer length.

433

434

435 **4 Thermosphere**

436

437 The research activity in the field of thermospheric long-term trends has been moderate. Out of five below  
438 cited papers three dealt with long-term trends in thermospheric density.

439 Weng et al. (2020) applied the machine-learning method to satellite drag data from a broad range of altitudes  
440 in the thermosphere to search for long-term trends in thermospheric density. Their trend estimates range from -  
441 1.5 to -2.0 %/decade between 250 and 575 km without any clear dependence on solar activity. They use S10.7  
442 instead of F10.7 to represent solar activity. Their model better captures thermospheric density during the deep  
443 solar minimum 2008-2009 than previous empirical models.

444 Mlynczak et al. (2022) used SABER/TIMED observations over 2002-2021 to study the behavior of the MLT  
445 region (heights of ~48-105 km, low and middle latitudes). They found significant cooling and contraction from  
446 2002 to 2019 (solar cycle minimum) due to weaker solar cycle and increasing CO<sub>2</sub>. This cooling and contraction  
447 of the MLT region contributes to decreasing thermospheric densities at LEO satellite orbits, where it results in  
448 increasing concentration of dangerous space debris.

449 WACCM-X global simulation of impact of increasing CO<sub>2</sub> concentration on thermospheric density under low  
450 solar activity conditions reveals a 27-30% decrease of atmospheric density at 400 km with respect to year 2000  
451 level if the Paris agreement surface warming limit 1.5°C is reached. This thermospheric density decrease will  
452 result in satellite and space debris orbital lifetime longer by 30% with consequent higher probability of  
453 dangerous satellite collisions with space debris (Brown et al., 2021). However, their neutral density trend at low  
454 solar activity is much higher than under medium and high solar activity conditions, and it is almost three times as  
455 high as the recent observational trends (e.g., Weng et al., 2020).

456 Liu et al. (2020) use GAIA model simulations to study the response of the thermosphere at heights of 100-  
457 400 km to CO<sub>2</sub> doubling. They found that the thermosphere will cool by 10 K, more near solstices than near  
458 equinoxes, more at summer pole than at winter pole. The meridional circulation shifts downward and strongly  
459 accelerates by 5-15 m/s. Semidiurnal tides are reduced by 40-60% in the whole thermosphere.

460 Perrone and Mikhailov (2019) inferred the atomic oxygen column content  $n[\text{O}]_{\text{col}}$  in June from June monthly  
461 medians of foF1 (critical frequency of F1 layer corresponding to its maximum electron density, height ~200 km)  
462 and foF2 (heights 250-300 km) of NH stations Rome (41.8°N, 12.5°E), Juliusruh (54.6°N, 13.4°E), Sodankylä  
463 (67.4°N, 26.6°E) and Boulder (40.0°N, 105.0°W) for six solar cycles (1958-2017). 93% of total variance of  
464  $n[\text{O}]_{\text{col}}$  is explained by the solar and geomagnetic activity. The linear trend for three midlatitude stations is  
465 negative but statistically insignificant, whereas Sodankylä reveals a statistically significant negative trend of  
466  $n[\text{O}]_{\text{col}}$  but this trend might be artifact due to not considering particle precipitation.

467

#### 468 **4.1 Summary**

469

470 The observed negative trend of thermospheric density about -2%/decade near 400 km continues without any  
471 evidence of clear dependence on solar activity, which is not consistent with model simulations under low solar  
472 activity conditions. The decrease in thermospheric density will result in increasing concentration of dangerous  
473 space debris on LEO (Low Earth Orbit) satellite orbits. GAIA model complex simulations of trends in many  
474 thermospheric parameters predict among others a downward shift and acceleration of meridional circulation and  
475 substantial reduction of semidiurnal tides; both have not yet been studied observationally. Perrone and Mikhailov

476 (2019) inferred negative trends of the atomic oxygen column content in June but their method might be  
477 questioned.

478

479

## 480 **5 Ionosphere**

481

482 Research activity in the field of ionosphere has been more intense than in the thermosphere. It has been  
483 focused on the F2 region, particularly on foF2 trends both due to importance of foF2 and availability of the  
484 longest and relatively reliable data sets. Some activity was also in the E-region ionosphere trend area. The first  
485 trend results were published for electron density in the topside ionosphere. On the other hand, there was little  
486 progress in the D-region trends since the review by Laštovička and Bremer (2004) and no activity in the previous  
487 five years.

488 Danilov and Konstantinova (2018) analyzed long-term trends in foE (typical heights ~110-115 km) for  
489 stations Juliusruh (54.6°N, 13.4°E) and Slough/Chilton over the period 1960-2010; they found trends -0.12 and -  
490 0.05 MHz/decade, respectively for yearly values and negative trends also for all months for the period after  
491 1980.

492 Danilov and Konstantinova (2019) analyzed long-term changes of foE from stations Juliusruh,  
493 Slough/Chilton, Rome (41.8°N, 12.5°E), Moscow (55.5°N, 37.3°E) and Wakkanai (45.2°N, 145.7°E) over the  
494 period 1960-2010. They found strong local-time dependence of foE trend for Juliusruh shown in Fig. 4 with  
495 positive trends in the morning sector, no trend at 11:00 LT and negative and stronger trends in the afternoon. The  
496 dependence of foE trend on LT is much weaker for Rome (lower latitude). Seasonally the trends reach maximum  
497 in December-January and minimum in July-August for Juliusruh (Fig. 4). The magnitude of foE trends clearly  
498 depends on geomagnetic latitude (Juliusruh and Slough/Chilton 54°N, Moscow 51°N, Rome 42°N and Wakkanai  
499 36°N); trend weakens with decreasing latitude. This finding according to Danilov and Konstantinova (2019)  
500 provides evidence supporting the impact of meridional transport of NO from auroral zone on the observed trends  
501 in foE.

502

### 503 **Figure 4.**

504

505 Givishvili and Leshchenko (2022) used data of Moscow and five Japanese stations to search for long-term  
506 trend in the E region response to solar flares over 1969-2015. From their analysis they derived the stable long-  
507 term increase of ratio of ionization rates  $q_x/(q_x + q_{EUV})$  in the E-region ( $q_x$  - soft X-ray ionization rate;  $q_{EUV}$  -  
508 solar EUV ionization rate) ; the ratio since 1969 approximately doubled in 2015. The increase was continuous,  
509 independent of solar cycle, season or latitude. 74 years of observations at Moscow provide small but  
510 insignificant increase of foE and relatively large and significant decrease of h'E (apparent height of the E-layer  
511 maximum).

512 The first results on long-term trends in the topside ionosphere based on DMSP (Defense Meteorological  
513 Satellite Program) satellite data over 1995-2017 were reported by Cai et al. (2019). They found the electron  
514 density trend near 860 km around 18:00 MLT (Magnetic Local Time) to have mean magnitude ranging from -2  
515 to +2 %/decade with a clear seasonal, latitudinal and longitudinal variation. The TIE GCM (Thermosphere-

516 Ionosphere-Electrodynamics General Circulation Model) simulated trends at 500 km have a similar geographic  
517 distribution at 18 MLT. Simulations also suggest that the predominant electron density trend driver at 500 km is  
518 the secular change of the Earth's magnetic field.

519 Zhou et al. (2022) investigated impact of increasing anthropogenic emissions on the occurrence of equatorial  
520 plasma bubbles (EPBs) via simulating the growth rate of the Rayleigh-Taylor instability, which is closely related  
521 to EPB generation. They used the Global Coupled Ionosphere-Thermosphere-Electrodynamics Model of the  
522 Institute of Geology and Geophysics, Chinese Academy of Sciences. With increasing CO<sub>2</sub> concentration the  
523 growth rate significantly increases at low altitudes below about 260 km, decreases at high altitudes above about  
524 320 km, and between 260 km and 320 km increases (decreases) before (after) midnight, indicating possible  
525 impact on radio communication systems. These changes are caused by gravity and electrodynamic term, not by  
526 neutral wind.

527 Zhang et al. (2018) found that the results of Perrone and Mikhailov (2017 – PM17) on exospheric  
528 temperature, which were based solely on foF1 measurements, were flawed and quantitatively unlikely. They also  
529 showed that the conclusions of PM17 on long-term analysis of ion temperatures derived from the incoherent  
530 scatter radar measurements are incorrect, partly due to misunderstanding of nature of the incoherent scatter radar  
531 measuring process.

532 The remaining papers deal with long-term trends in the F2-region, mainly in foF2 but partly also in hmF2.

533 An analysis of a 70-years long homogenized series (1947-2017) of observations of ionosonde at Wuhan  
534 (30°N, central China) by Yue et al. (2018) found a weak but statistically significant average negative trend in  
535 foF2, -0.021 MHz/decade, which varied with local time from negative to slightly positive. The observed trends  
536 are attributed primarily to the secular change of the Earth's magnetic field with CO<sub>2</sub> being the second important  
537 driver. As for hmF2, the average trend is -1.06 km/decade; the roles of CO<sub>2</sub> and Earth's magnetic field in this  
538 trend are comparable (Yue et al., 2018).

539 Sharan and Kumar (2021) examined long-term foF2 variations from SH stations Hobart, Canberra (35.3°S,  
540 149.1°E) and Christchurch (43.5°S, 172.6°E) over 1947-2006. They found a decrease of foF2 by 0.1-0.4 MHz  
541 per five solar cycles mainly due to increasing concentration of CO<sub>2</sub>; the midday trends were more significant and  
542 agreed better with model-inferred expectations than midnight trends.

543 When the solar cycle 24 is included into nighttime foF2 long-term trends for stations Wakkanai (45.4°N,  
544 141.7°E) and Kokubunji (35.7°N, 139.5°E), the trends become less negative, likely due to application of F10.7 as  
545 solar activity proxy (De Haro Barbas et al., 2020). The trend weakening is less pronounced when Mg II is used  
546 as solar activity proxy instead of F10.7.

547 Danilov and Konstantinova (2020c) found for Juliusruh that the pronounced negative trends of hmF2 and  
548 foF2 persisted until 2002-2003, then they were followed by a vague period with chaotic changes and in the most  
549 recent years a negative trend appeared again.

550 Sergeenko (2021) analyzed significant deviations (>20%) of foF2 ( $\Delta$ foF2) from 10-day  
551 median for stations Moscow (55.5°N, 37.3°E), Slough/Chilton (51.5°N, 01°W) and Hobart (42.9°S, 147.3°E) for  
552 the period 1948-2010. They found that the maximum amplitudes of positive  $\Delta$ foF2 increased since the early  
553 1980s at all stations in winter and except Moscow also in summer, whereas for negative  $\Delta$ foF2 there was no  
554 change in Chilton and Hobart and some increase in Moscow (particularly in summer). The increasing trend in  
555 positive  $\Delta$ foF2 is likely related to changes in thermospheric wind system (Sergeenko, 2021).

556

## 557 **5.1 Summary**

558

559 Significant progress was reached in long-term trends in the E-region ionosphere, namely in foE. These trends  
560 were found to depend principally on local time up to their sign; this dependence is strong at European high  
561 midlatitudes but much less pronounced at European low midlatitudes, it is stronger in winter than in summer.  
562 Trends in foE also weaken with decreasing geomagnetic latitude of station.

563 In the ionospheric F2-region very long data series (starting at 1947) of foF2 at NH as well as SH revealed  
564 very weak but statistically significant negative trends. Some problems with foF2 and hmF2 trends were indicated  
565 in solar cycle 24 (e.g., Haro Barbas et al., 2022), and around the solar cycle minimum 23/24 (e.g., Danilov and  
566 Konstantinova, 2020c).

567 First results on long-term trends in the topside ionosphere electron densities (trends ranging from -2 to +2  
568 %/decade at 840 km) and in the equatorial plasma bubbles (height-dependent sign of trends) were reported.

569 The role of secular change of the Earth's magnetic field in long-term trends in F2 region has also been studied  
570 but these results are reported in section 7. The results on selection of the optimum solar activity proxies for F2  
571 region trend studies are reported in section 2.

572

573

## 574 **6 Global or Very-Long-Term Modeling**

575

576 Solomon et al. (2019) realized the first global simulation with model WACCM-X of changes of temperature  
577 excited by anthropogenic trace gases simultaneously from surface to the base of exosphere. They found that the  
578 anthropogenic cooling begins in the lower stratosphere and it becomes dramatic, almost -2 K/decade, for the  
579 global mean zonal mean temperature in the thermosphere. Only near the mesopause (~85-90 km) the cooling  
580 approaches zero values. This pattern qualitatively agrees with observations. The temperature trend in the  
581 thermosphere is somewhat stronger in the solar cycle minimum compared to the solar cycle maximum  
582 conditions, likely due to the stronger solar cycle variation of NO and O(<sup>3</sup>P) infrared irradiance compared to that  
583 of CO<sub>2</sub>, which results in a relatively larger role of CO<sub>2</sub> in the solar activity minimum conditions.

584 Cnossen (2022) used model WACCM-X to simulate climate change in the upper atmosphere (90-500 km) for  
585 the period 1950-2070 with moderate emission scenario SSP2-4.5 (Shared Socio-economic Pathway), secular  
586 change of the Earth magnetic field and reasonable solar radiative and particle forcing in order to get the climate  
587 projection into the 21<sup>st</sup> century. The obtained trends of thermospheric temperature (cooling) and density  
588 (reduction) are twice as large in 2015-2070 compared to the period 1950-2007 due to the more rapid absolute  
589 increase of CO<sub>2</sub> concentration. Trends in ionospheric parameters also become substantially stronger. However,  
590 they display considerable spatial variability due to the secular change of the Earth's magnetic field. The strongest  
591 ionospheric changes are expected in the region of 50°S-20°N and 90°-0°W.

592 Yue et al. (2022) for the first time expanded simulations of the ionosphere over the whole Holocene (9455  
593 BCE – 2015 CE) with the Coupled Ionosphere-Thermosphere- Electrodynamics model of the Chinese Institute  
594 of Geology and Geophysics driven by realistic geomagnetic field, CO<sub>2</sub> levels and solar activity. They found that  
595 oscillations of the global mean ionospheric profile are characterized by effects of geomagnetic field, decrease

596 (increase) of electron density above (below) ~200 km due to increasing CO<sub>2</sub> concentration, and violent  
597 oscillations in phase with solar activity; the corresponding contributions to overall variability being about 20%,  
598 20% and 60%, respectively. The CO<sub>2</sub> effect is becoming non-negligible and significant after ~1800 CE. The  
599 increase of CO<sub>2</sub> by 400 ppmv resulted in simulated decrease of foF2 by 1.2 MHz, hmF2 by 34 km, and TEC by 4  
600 TECU.

601 Garcia et al. (2019) simulated middle atmosphere temperature trends in the 20<sup>th</sup> and 21<sup>st</sup> centuries with model  
602 WACCM. They investigated bi-decadal changes of temperature trend profiles with the RCP 6.0 scenario of the  
603 greenhouse gas concentration evolution and found the biggest change between 1975-1995 and 1995-2015, which  
604 is attributed to loss and recovery of stratospheric ozone due to changing emissions of anthropogenic halogens.  
605 After 2015 the development of profile of temperature trends is controlled mainly by non-ODS greenhouse gases.

606

### 607 **6.1 Summary**

608 Trends in temperature in the whole atmosphere from surface to the exosphere were simultaneously simulated  
609 for the first time; in individual layers they reasonably agree with other results. The simulation confirmed the  
610 observed height-dependent pattern of trends. Very long-period simulations of the middle atmosphere,  
611 thermosphere and ionosphere confirmed acceleration of the trends during the last several decades, specified role  
612 of ozone-depleting substances, and it provided the first information about possible trends over the whole  
613 Holocene.

614

615

## 616 **7 Non-CO<sub>2</sub> Drivers of Trends**

617

618 The increasing concentration of greenhouse gases (GHGs, mainly CO<sub>2</sub>) is not the only driver of long-term  
619 trends in the upper atmosphere (e.g., Laštovička, 2017). At present the effect of secular change of Earth's  
620 magnetic field and anthropogenic changes of stratospheric ozone are considered to be the most important  
621 additional trend drivers in the ionosphere-thermosphere-mesosphere system. Other driver's roles are also  
622 discussed, e.g. geomagnetic activity, atmospheric waves coming from below, or water vapor (only in the  
623 mesosphere). Solar activity also changes on long-term scales but because we need to remove solar cycle effect  
624 from (particularly ionospheric) data before calculating trends, the solar activity effect is largely removed from  
625 trend calculations. Let us start with the secular change of magnetic field, because its effects were relatively  
626 broadly studied in the period 2018-2022.

627 Cnossen (2020) performed a long-term (1950-2015) simulation of the upper atmosphere with model  
628 WACCM-X with realistic variation of solar and geomagnetic activity, changes of the main magnetic field, and  
629 trace gas emissions including CO<sub>2</sub>. The results confirm that CO<sub>2</sub> is the main driver of trends in thermospheric  
630 temperature and density, even though at high magnetic latitudes the secular change of geomagnetic field plays  
631 also a role, particularly at NH. Spatial patterns of trends in hmF2, NmF2 and TEC indicates the superposition of  
632 effects of CO<sub>2</sub> and secular change of geomagnetic field, the latter being dominant in about 50°S-20°N and 60°W-  
633 20°E. This longitudinal sector experiences the largest change of the magnetic equator position (e.g., Cnossen,  
634 2020).



635 Qian et al. (2021) simulated long-term trends in the upper atmosphere using model WACCM-X. They found  
636 that trends caused by both the secular change of geomagnetic field but also the increasing concentration of CO<sub>2</sub>  
637 exhibit significant latitudinal and longitudinal variability, which was not expected for CO<sub>2</sub>. Thermospheric  
638 trends in density and temperature are quite predominantly driven by greenhouse gases (GHGs); the secular  
639 change of geomagnetic field plays some role in temperature trends in 120°W-20°E. In this longitudinal sector,  
640 the secular change of geomagnetic field plays comparable role with GHGs in trends in hmF2, NmF2 and Te  
641 (electron temperature) and in Ti (ion temperature) above 320 km while below 320 km the Ti trend is dominated  
642 by GHGs. Figure 5 shows the changes of neutral density, neutral temperature Tn, Te and Ti from the 1960s to  
643 the 2010s. The neutral temperature and density change is clearly dominated by GHGs, whereas in Te and Ti in  
644 some regions the effect of the secular change of magnetic field plays the dominant role. The secular change of  
645 geomagnetic field is an important driver in sector 120°W-20°E but it excites locally both positive and negative  
646 trends, consequently in global average trends its contribution is negligible.

647

#### 648 **Figure 5**

649

650 Simulations with the TIE GCM model (Cai et al., 2019) suggest that the predominant electron density trend  
651 driver at 500 km is the secular change of the Earth's magnetic field.

652 During the next 50 years the dipole momentum of the Earth's magnetic field is predicted to decrease by  
653 ~3.5%, the South Atlantic magnetic anomaly will expand, deepen and drift westward, and magnetic dip poles  
654 will also move, which according to simulations with model TIE-GCM will have impact on the thermosphere-  
655 ionosphere changes from 2015 to 2065 (Cnossen and Maute, 2020). The global mean thermospheric density  
656 should slightly increase by ~1% in average and by up to 2% during magnetically disturbed conditions ( $K_p \geq 4$ ),  
657 particularly at SH. Global TEC should changes in the range -3% to +4% pending on season and UT but regional  
658 changes may be up to  $\pm 35\%$  in 45°S-45°N, 110°W-0°W during daytime, mainly due to changes in the vertical  $\mathbf{E}$   
659  $\times \mathbf{B}$  drift (vector product of electric and magnetic field is a plasma drift perpendicular to them). The equatorial  
660 ionization anomaly will weaken in sector ~105-60°W. The predicted changes of neutral density are very small  
661 compared to effects of other trend drivers (mainly CO<sub>2</sub>) but the predicted changes in TEC might be regionally  
662 substantial.

663 As concerns observational results, Yue et al. (2018) found a weak but statistically significant average negative  
664 trend in foF2 from 70 years of data at Wuhan (central China), which they attributed primarily to the secular  
665 change of the Earth's magnetic field with CO<sub>2</sub> being the second important driver.

666 Other discussed topic is the impact of geomagnetic activity on CO<sub>2</sub>-driven trends in the thermosphere and  
667 ionosphere. One paper dealt with long-term changes in NO radiative cooling of the thermosphere.

668 Liu et al. (2021) used model GAIA to simulate the impact of geomagnetic activity on CO<sub>2</sub>-driven trends in  
669 the thermosphere and ionosphere. They found that the thermospheric density is the most robust indicator of the  
670 effect of CO<sub>2</sub>. The geomagnetic activity can either weaken or strengthen CO<sub>2</sub>-driven trends in hmF2 and NmF2  
671 depending on time and latitude. There is interdependency between forcing by CO<sub>2</sub> and by geomagnetic activity;  
672 the efficiency of CO<sub>2</sub> forcing is higher under low geomagnetic activity forcing than under high levels of  
673 geomagnetic activity forcing, and under conditions of high CO<sub>2</sub> concentration the geomagnetic forcing is more  
674 efficient.

675 Chen et al. (2022) found that the geomagnetic activity-induced long-term change of foF2 is seasonally  
676 discrepant. With long-term increase of geomagnetic activity foF2 increases in winter while decrease in summer  
677 at middle and low latitudes; foF2 decreases at higher latitudes whereas turns to increases with decreasing latitude  
678 in equinox. The linear trend component is dominated by a long-term decreasing trend, which is in line with the  
679 increasing greenhouse gas concentration. The geomagnetic activity in the most recent decades has a decreasing  
680 trend, which has to be considered when the linear trend of foF2 is calculated to estimate the impact of  
681 greenhouse gases.

682 Lin and Deng (2019) studied the role of NO in the climatology of global energy budget and found that from  
683 1982 to 2013 the decadal change of NO cooling reached ~25% of change of total heating in the thermosphere  
684 below 150 km (its importance decreases with increasing height) based on simulations with the Global  
685 Ionosphere-Thermosphere Model (GITM; simulations were run for constant CO<sub>2</sub>). However, the decadal change  
686 of NO cooling was mainly due to decreasing solar (F10.7) and geomagnetic (Ap) activities.

687

## 688 **7.1 Summary**

689

690 The main activity was focused on the role of the secular change of the main magnetic field of Earth. Model  
691 simulations show that its role in long-term trends is most important (comparable or even higher than the role of  
692 GHGs) in ionospheric parameters hmF2, foF2, TEC (total electron content) electron temperature and partly ion  
693 temperature in the region of about 50°S-20°N and 20°E-110°W (various simulations provide somewhat different  
694 longitudinal range), while its role in neutral atmosphere parameters, density and temperature is much smaller,  
695 almost negligible. In global average trends, however, the role of secular change of magnetic field is negligible  
696 even in ionospheric parameters; it excites locally both positive and negative trends (Qian et al., 2021). On the  
697 other hand, trends in electron density well in the topside ionosphere (~500-850 km) appear to be controlled by  
698 the secular change of geomagnetic field.

699 Model simulations by Liu et al. (2021) reveal that the geomagnetic activity, another potential driver of long-  
700 term trends particularly in the ionosphere, can either weaken or strengthen CO<sub>2</sub>-driven trends in hmF2 and  
701 NmF2 depending on time and latitude.

702

703

## 704 **8 Conclusions**

705

706 This article reviews progress in long-term trends in the mesosphere-thermosphere-ionosphere system reached  
707 over the period 2018-2022. Overall this progress may be considered significant. The most active research was  
708 reached in the area of trends in the mesosphere and lower thermosphere (MLT). Also research areas of problems  
709 in trend calculations, global modeling and non-CO<sub>2</sub> drivers of long-term trends have been reviewed. The main  
710 results are as follows:

711 Trends in the MLT region were relatively broadly studied. The contradictions about long-term trends of  
712 concentration of CO<sub>2</sub> derived from satellite measurements were finally solved, which is the result of principal  
713 importance. It was found that the CO<sub>2</sub> concentration trends in the MLT region below 90 km do not differ  
714 statistically from trends at surface, even though they appear to be slightly larger at heights above 90 km. The  
715 most studied parameter was temperature. Huang and Mayr (2021) found that trends might significantly vary with  
716 local time and height in the whole height range of 30-110 km but they studied data series only 13 years long.  
717 However, She et al. (2019) claim that data sets longer than two solar cycles are necessary to obtain reliable long-  
718 term temperature trend. Model simulations confirm general cooling, even though the WACCM simulations by  
719 Qian et al. (2019) indicate that the temperature trend becomes near zero or even slightly positive in the summer  
720 upper mesosphere, likely due to dynamic effects. The results on temperature trends are generally consistent with  
721 older results but were developed and detailed further.

722 Other important group in the MLT region is dynamical parameters, winds and atmospheric waves. Here the  
723 trend pattern is much more complex. Observational data indicate different wind trends up to sign of trend in  
724 different geographic regions, which is supported by model simulations. The limited activity in the area of  
725 atmospheric waves was concentrated on tides. Meteor radar wind data from high/middle latitudes revealed no  
726 significant trend in diurnal tides and changes of semidiurnal tide, which differ according to altitude and latitude.  
727 On the other hand, simulations with WACCM6 provide positive trends for both migrating and non-migrating  
728 diurnal tides. Water vapor concentration trends in the mesosphere are generally positive, only in the equatorial  
729 region there is almost no trend. As for long-term trends in the related noctilucent clouds (NLCs), water vapor  
730 concentration was found to be the main driver of trends in brightness and occurrence frequency, whereas cooling  
731 through mesospheric shrinking is responsible for slight decrease in NLC heights. The polar mesospheric summer  
732 echo trend was found to be positive, which might be related to the observed negative trend of mesospheric  
733 temperatures in polar latitudes.

734 The research activity in the thermosphere was substantially lower. The negative trend of thermospheric  
735 density continues without any evidence of clear dependence on solar activity. The decrease in thermospheric  
736 density will result in increasing concentration of dangerous space debris on LEO (Low Earth Orbit) satellite  
737 orbits. GAIA model simulations of trends in many thermospheric parameters predict among others a downward  
738 shift and acceleration of meridional circulation and substantial reduction of semidiurnal tides; both have not yet  
739 been studied observationally.

740 Significant progress was reached in long-term trends in the E-region ionosphere, namely in foE. These trends  
741 were found to depend principally on local time up to their sign; this dependence is strong at European high  
742 midlatitudes but much less pronounced at European low midlatitudes. In the ionospheric F2-region very long  
743 data series (starting at 1947) of foF2 at NH as well as SH revealed very weak but statistically significant negative  
744 trends. Some problems with foF2 and hmF2 were indicated in solar cycle 24, particularly towards its end. First  
745 results on long-term trends were reported for two new parameters, the topside ionosphere electron densities (near  
746 840 km) and the equatorial plasma bubbles.

747 An important part of the investigation of long-term trends is the specification of the roles of individual trend  
748 drivers. The most important driver is the increasing concentration of CO<sub>2</sub> but other drivers also play a role. The  
749 most studied one in the last five years was the effect of the secular change of the Earth's magnetic field. The  
750 results of extensive modeling are mutually qualitatively consistent. They reveal the dominance of secular

751 magnetic change in trends in foF2, hmF2, TEC and Te in the sector of about 50°S-20°N and 110°W-20°E  
752 (longitudinal extent in different simulations differs). However, its effect is locally both positive and negative, so  
753 in the global average this effect is negligible. In the neutral atmosphere parameters the effects of the secular  
754 change of Earth's magnetic field are much smaller. Model simulations of the geomagnetic activity impact show  
755 that it can either weaken or strengthen CO<sub>2</sub>-driven trends in hmF2 and NmF2 depending on time and latitude and  
756 that its effect is seasonally discrepant.

757 Modeling provided some results not included in topical sections. Solomon et al. (2019) realized the first  
758 global simulation with model WACCM-X of changes of temperature excited by anthropogenic trace gases  
759 simultaneously from the Earth's surface to the base of exosphere. The results are generally consistent with  
760 observational pattern of trends. Very long-term modeling yields trends of thermospheric temperature and  
761 density, which are twice as large in the 21<sup>st</sup> century as trends in historical period due to more rapid absolute  
762 increase of CO<sub>2</sub> concentration. Simulation of ionospheric trends over the whole Holocene was reported for the  
763 first time.

764 There are various problems in calculating long-term trends. They can be divided into three groups: (1)  
765 natural variability, (2) data problems, and (3) methodology. These problems were reviewed by Laštovička and  
766 Jelínek (2019). Main progress in the last five years was reached by shedding light on problems related to natural  
767 variability, mainly on the problem of the removal/suppression of the effect of the solar cycle using various solar  
768 activity proxies, and also in specifying problems of solar cycle 24 (2009-2019).

769 New findings contribute to improvement and broadening of scenario of long-term trends in the upper  
770 atmosphere and ionosphere. Time is approaching when it will be possible to construct a joint trend scenario of  
771 trends in the stratosphere-mesosphere-thermosphere-ionosphere system.

772 Despite evident progress having been made, it is clear that various challenges and open problems still  
773 remain. The key problem is the long-term trends in dynamics, particularly in the activity of atmospheric waves,  
774 which are a very important component of vertical coupling in the atmosphere and which affect all layers of the  
775 upper atmosphere. At present we only know that these trends might be regionally different, even opposite. The  
776 atmospheric wave activity trend pattern seems to be complex and the amount of observational data and also of  
777 studies dealing with wave trends is insufficient. There are also challenges in further improvement of models for  
778 long-term trend investigations and their interpretation. There is for example a difference in thermospheric neutral  
779 density trends under low solar activity conditions between observations and simulations; these trends affect  
780 lifetimes of dangerous space debris. Long-term trend in TEC with implications to GNSS signal propagation and  
781 its applications in positioning and other areas is not well known and understood and related trends in ionospheric  
782 scintillations are not known at all. The role of majority potential non-CO<sub>2</sub> drivers of long-term trends in the  
783 upper atmosphere is known only very qualitatively and needs to be better specified. Various water vapor  
784 observational and model trends are still not in consistent agreement with one another. Trends in various  
785 parameters depend on local time and season, which has not been sufficiently studied. In summary, although there  
786 has been significant progress made in studies published between 2018-2022, it is clear that there is still much  
787 work to be done in reaching scientific closure on these outstanding issues.

788

789

790 **Data availability.** No data sets were used in this article.

791  
792  
793  
794  
795  
796  
797  
798  
799  
800  
801  
802  
803  
804  
805  
806  
807  
808  
809  
810  
811  
812  
813  
814  
815  
816  
817  
818  
819  
820  
821  
822  
823  
824  
825  
826  
827  
828  
829

**Competing interest.** The author has no competing interests.

**Financial support.** This research has been supported by the Czech Science Foundation under grant 21-03295S.

## References

Aikin, A. C., Chanin, M. L., Nash, J., and Kendig, D. J.: Temperature trends in the lower mesosphere. *Geophys. Res. Lett.*, 18, 416-419, 1991.

Ardalan, M., Keckhut, P., Hauchecorne, A., Wing, R., Meftah, M., and Farhani, G.: Updated climatology of mesospheric temperature inversions detected by Rayleigh lidar above Observatoire de Haute Provence, France, using a K-mean clustering technique, *Atmosphere*, 13(5), #814, <https://doi.org/10.3390/atmos13050814>, 2022.

Bailey, S. M., Thurairajah, B., Hervig, M. E., Siskind, D. E., Russell, J. M. III, and Gordley, L. L.: Trends in the polar summer mesosphere temperature and pressure altitude from satellite observations, *J. Atmos. Sol.-Terr. Phys.*, 220, 105650, <https://doi.org/10.1016/j.jastp.2021.105650>, 2021.

Bizuneh, C. L., Prakash Raju, U. J., Nigussie, M., and Guimaraes Santos, C. A.: Long-term temperature and ozone response to natural drivers in the mesospheric regions using 16 years (2005-2022) of TIMED/SABER observation data at 5-15°N, *Adv. Space Res.*, 70, 2095-2111, <https://doi.org/10.1016/j.asr.2022.06.051>, 2022.

Brown, M. K., Lewis, H. G., Kavanagh, A. J., and Cnossen, I.: Future decreases in thermospheric neutral density in low Earth orbit due to carbon dioxide emissions, *J. Geophys. Res. Atmos.*, 126(8), e2021JD034589, <https://doi.org/10.1029/2021JD034589>, 2021.

Cai, Y., Yue, X., Wang, W., Zhang, S.-R., Liu, L., Liu, H., and Wan, W.: Long-term trend of topside electron density derived from DMSP data during 1995-2017, *J. Geophys. Res. Space Phys.*, 124, 10708-10727, <https://doi.org/10.1029/2019JA027522>, 2019.

Chen, Y., Liu, L., Le, H., Zhang, H., and Zhang, R.: Seasonally discrepant long-term variations of the F2-layer due to geomagnetic activity and modulation to linear trend, *J. Geophys. Res. Space Phys.*, 127(11), e2022JA030951, <https://doi.org/10.1029/2022JA030951>, 2022.

Cicerone, R. J.: Greenhouse cooling up high. *Nature*, 344, 104-105, 1990.

Cnossen, I.: Analysis and attribution of climate change in the upper atmosphere from 1950 to 2015 simulated by WACCM-X. *J. Geophys. Res. Space Phys.*, 125(12), e2020JA028623, <https://doi.org/10.1029/2020JA028623>, 2020.

Cnossen, I.: A realistic projection of climate change in the upper atmosphere into the 21<sup>st</sup> century, *Geophys. Res. Lett.*, 49(19), e2022GL100693, <https://doi.org/10.1029/2022GL100693>, 2022.

Cnossen, I., and Maute A.: Simulated trends in the ionosphere-thermosphere climate due to predicted main magnetic field changes from 2015 to 2065. *J. Geophys. Res. Space Phys.*, 125(3), e2019JA027738, <https://doi.org/10.1029/2019JA027738>, 2020.

830 Dalla Santa, K., Orbe, C., Rind, D., Nazarenko, L., and Jonas, J.: Dynamical and trace gas responses of the  
831 quasi-biennial oscillation to increased CO<sub>2</sub>, *J. Geophys. Res. Atmos.*, 126(8), e2020JD034151,  
832 <https://doi.org/10.1029/2020JD034151>, 2021.

833 Dalin, P., Perminov, V., Pertsev, N., and Romejko, V.: Updated long-term trends in mesopause temperature,  
834 airglow emissions, and noctilucent clouds, *J. Geophys. Res. Atmos.*, 125(5), e2019JD030814,  
835 <https://doi.org/10.1029/2019JD030814>, 2020.

836 Danilov, A. D. Behavior of F2 region parameters and solar activity indices in the 24<sup>th</sup> cycle, *Adv. Space Res.*, 67,  
837 102-110, <https://doi.org/10.1016/j.asr.2020.09.042>, 2021.

838 Danilov, A. D., and Berberova, N. A.: Some applied aspects of the study of trends in the  
839 upper and middle atmosphere, *Geomagn. Aeron.*, 61, 578-588, <https://doi.org/10.1134/S0016793221040046>,  
840 2021.

841 Danilov, A. D., and Konstantinova, A. V.: Long-term trends in the critical frequency of the E-layer, *Geomagn.*  
842 *Aeron.*, 58, 338-347, doi: 10.1134/S0016793218030052, 2018.

843 Danilov, A. D., and Konstantinova, A. V.: Diurnal and seasonal variations in long-term changes in the E-layer  
844 critical frequency, *Adv. Space Res.*, 63, 359-370, <https://doi.org/10.1016/j.asr.2018.10.015>, 2019.

845 Danilov, A. D., and Konstantinova, A. V.: Long-term variations of the parameters of the middle and upper  
846 atmosphere and ionosphere (review), *Geomagn. Aeron.*, 60, 397-420,  
847 <https://doi.org/10.1134/S0016793220040040>, 2020a.

848 Danilov, A. D., and Konstantinova, A. V.: Trends in parameters of the F2 layer and the 24<sup>th</sup> solar activity cycle,  
849 *Geomagn. Aeron.*, 60, 586-596, <https://doi.org/10.1134/s0016793220050047>, 2020b.

850 Danilov, A. D., and Konstantinova, A. V.: Trends in hmF2 and the 24<sup>th</sup> solar activity cycle, *Adv. Space Res.*, 66,  
851 292-298, <https://doi.org/10.1016/j.asr.2020.04.011>, 2020c.

852 Das, U.: Spatial variability in long-term temperature trends in the middle atmosphere from SABER/TIMED  
853 observations, *Adv. Space Res.*, 68, 2890-2903, <https://doi.org/10.1016/j.asr.2021.05.014>, 2021.

854 De Haro Barbas, B. F., Elias, A. G., Fagre, M., and Zossi, B. S.: Incidence of solar cycle 24 in nighttime foF2  
855 long-term trends for two Japanese ionospheric stations, *Studia Geoph. Geod.*, 64, 407-418,  
856 <https://doi.org/10.1007/s11200-021-0584-9>, 2020.

857 Elias, A. G., De Haro Barbas, B. F., Zossi, B. S., Medina, F. D., Fagre, M., and Venchiaerutti, J. V.: Review of  
858 long-term trends in the equatorial ionosphere due to geomagnetic field secular variations and its relevance  
859 to space weather, *Atmosphere*, 13, #40, <https://doi.org/10.3390/atmos13010040>, 2022.

860 Emmert, J. T., Picone, J. M., and Meier, R. R.: Thermospheric global average density trends 1967-2007, derived  
861 from orbits of 5000 near-Earth objects. *Geophys. Res. Lett.*, 35, L05101 (2008), doi:  
862 10.1029/2007GL032809.

863 French, W. J. R., Mulligan, F. J., and Klekociuk, A. R.: Analysis of 24 years of mesopause region OH rotational  
864 temperature observations at Davis, Antarctica – Part 1: long-term trends, *Atmos. Chem. Phys.*, 20, 6379-  
865 6394, <https://doi.org/10.5194/acp-20-6379-2020>, 2020.

866 Garcia, R. R., Yue, J., and Russell, J. M. III.: Middle atmosphere temperature trends in the twenties and twenty-  
867 first centuries simulated with the Whole Atmosphere Community Climate Model (WACCM), *J. Geophys.*  
868 *Res. Space Phys.*, 124, 7984-7993, <https://doi.org/10.1029/2019JA026909>, 2019.

869 Givishvili, G. V., and Leshchenko, L. N.: Long-term trend of the ionospheric E-layer response to solar flares,  
870 Sol.-Terr. Phys., 8, 51-57, <https://doi.org/10.12737/stp-81202206>, 2022.

871 Huang, F. T., and Mayr, H. G.: Temperature decadal trends, and their relations to diurnal variations in the lower  
872 thermosphere, stratosphere and mesosphere, based on measurements from SABER on TIMED. Ann.  
873 Geophys., 39, 327-339, <https://doi.org/10.5194/angeo-39-327-2021>, 2021.

874 Huang, J., Hao, Y., Zhang, D., and Xiao, Z.: The use of monthly mean average for investigating the presence of  
875 hysteresis and long-term trends in ionospheric NmF2. J. Geophys. Res. Space Phys., 125(1),  
876 e2019JA026905, <https://doi.org/10.1029/2019JA026905>, 2020.

877 Huang, T.-Y.: Influences of CO<sub>2</sub> increase, solar cycle variation, and geomagnetic activity on airglow from 1960-  
878 2015, J. Atmos. Sol.-Terr Phys., 171, 164-175, <https://doi.org/10.1016/j.jastp.2017.06.008>, 2018.

879 Jaen, J., Renkwitz, T., Chau, J. L., He, M., Hoffmann, P., Yamazaki, Y., Jacobi, C., Tsutsumi, M., Matthias, V.,  
880 and Hall, C.: Long-term studies of mesosphere and lower thermosphere summer length definitions based on  
881 mean zonal wind features observed for more than one solar cycle at middle and high latitudes in the  
882 Northern Hemisphere, Ann. Geophys., 40, 23-35, <https://doi.org/10.5194/angeo-40-23-2022>, 2022.

883 Kuilman, M. S., Zhang, Q., Cai, M., and Weng, Q.: Using the climate feedback response analysis method to  
884 quantify climate feedbacks in the middle atmosphere, Atmos. Chem. Phys., 20, 12409-12430,  
885 <https://doi.org/10.5194/acp-20-12409-2020>, 2020.

886 Kogure, M., Liu, H., and Tao, C.: Mechanisms for zonal mean wind responses in the thermosphere to doubled  
887 CO<sub>2</sub> concentration, J. Geophys. Res. Space Phys., 127(9), e2022JA030643,  
888 <https://doi.org/10.1029/2022JA030643>, 2022.

889 Lainer, M., Hocke, K., Eckert, E., and Kämpfer, N.: Significant decline of mesospheric water vapor at the  
890 NDACC site near Bern in the period 2007 to 2018, Atmos. Chem. Phys., 19, 6611-6620,  
891 <https://doi.org/10.5194/acp-19-6611-2019>, 2019.

892 Latteck, R., Renkwitz, T., and Chau, J. L.: Two decades of long-term observations of polar mesospheric echoes  
893 at 69°N, J. Atmos. Sol.-Terr. Phys., 216, 105576, <https://doi.org/10.1016/j.jastp.2021.105576>, 2021.

894 Laštovička, J.: A review of recent progress in trends in the upper atmosphere. J. Atmos. Solar- Terr. Phys., 163,  
895 2–13, <https://doi.org/10.1016/j.jastp.2017.03.009>, 2017.

896 Laštovička, J.: Is the relation between ionospheric parameters and solar proxies stable? Geophys. Res. Lett.,  
897 46, 14208-14213, <https://doi.org/10.1029/2019GL085033>, 2019.

898 Laštovička, J.: What is the optimum solar proxy for long-term ionospheric investigations? Adv. Space Res., 67,  
899 2-8, <https://doi.org/10.1016/j.asr.2020.07.025>, 2021a.

900 Laštovička, J.: The best solar activity proxy for long-term ionospheric investigations. Adv. Space Res., 68, 2354-  
901 2360. <https://doi.org/10.1016/j.asr.2021.06.032>, 2021b.

902 Laštovička, J.: Long-term changes of ionospheric climate in terms of foF2. Atmosphere, 13:110,  
903 <https://doi.org/10.3390/atmos13010110>, 2022.

904 Laštovička, J., Akmaev, R. A., Beig, G., Bremer, J., and Emmert, J. T.: Global change in the upper atmosphere.  
905 Science, 314, 1253-1254, 2006.

906 Laštovička, J., Akmaev, R. A., Beig, G., Bremer, J., Emmert, J. T., Jacobi, C., Jarvis, M. J., Nedoluha, G.,  
907 Portnyagin, Yu. I., and Ulich, T.: Emerging pattern of global change in the upper atmosphere and ionosphere.  
908 Ann. Geophysicae, 26, 1255-1268, <https://doi.org/10.5194/angeo-26-1255-2008>, 2008.

909 Laštovička, J., Bremer, J.: An overview of long-term trends in the lower ionosphere below 120 km. *Surv.*  
910 *Geophys.*, 25, 69–99, <https://doi.org/10.1023/B:GEOP.0000015388.75164.e2>, 2004.

911 Laštovička, J., Jelínek, Š.: Problems in calculating long-term trends in the upper atmosphere. *J. Atmos. Solar-*  
912 *Terr. Phys.*, 189, 80-86, <https://doi.org/10.1016/j.jastp.2019.04.011>, 2019.

913 Laštovička, J., and Pancheva, D.: Changes in characteristics of planetary waves at 80-100 km over Central and  
914 Southern Europe since 1980. *Adv. Space Res.*, 11 (3), 31-34, 1991.

915 Li, T., Yue, J., Russell J. M. III, and Zhang, X.: Long-term trend and solar cycle in the middle atmosphere  
916 temperature revealed from merged HALOE and SABER datasets. *J. Atmos. Sol.-Terr. Phys.*, 212, 105506,  
917 <https://doi.org/10.1016/j.jastp.2020.105506>, 2021.

918 Lin, C.-Y., and Deng, Y.: Nitric oxide in climatological energy budget during 1982-2013. *J. Geophys. Res.*  
919 *Space Phys.*, 124, 782-789, <https://doi.org/10.1029/2018JA025902>, 2019.

920 Liu, H., Tao, C., Jin, H., and Nakamoto, Y.: Circulation and tides in a cooler upper atmosphere: Dynamical  
921 effects of CO<sub>2</sub> doubling, *Geophys. Res. Lett.*, 47(10), e2020GL087413,  
922 <https://doi.org/10.1029/2020GL087413>, 2020.

923 Liu, H., Tao, C., Jin, H., and Abe, T.: Geomagnetic activity effect on CO<sub>2</sub>-driven trend in the thermosphere and  
924 ionosphere: Ideal model experiments with GAIA. *J. Geophys. Res. Space Phys.*, 126(1), e2020JA028607,  
925 <https://doi.org/10.1029/2020JA028607>, 2021.

926 Lübken, F.-J., Berger, U., and Baumgarten, G.: On the anthropogenic impact on long-term evolution of  
927 noctilucent clouds, *Geophys. Res. Lett.*, 45, 6681-6689, <https://doi.org/10.1029/2918GL077719>, 2018.

928 Lübken, F.-J., Baumgarten, G., and Berger, U.: Long-term trends of mesospheric ice layers” A model study, *J.*  
929 *Atmos. Sol.-Terr. Phys.*, 214, 105378, <https://doi.org/10.1016/j.jastp.2020.105378>, 2021.

930 Mlynczak, M. G., Hunt, L. A., Garcia, R. R., Harvey, V. L., Marshall, B. T., Yue, J., Mertens, C. J., and Russell,  
931 J. M. III: Cooling and contraction of the mesosphere and lower thermosphere from 2002 to 2021, *J.*  
932 *Geophys. Res. Atmos.*, 127(22), e2022JD036767, <https://doi.org/10.1029/2022JD036767>, 2022.

933 Nedoluha, G. E., Gomez, R. M., Boyd, I., Neal, H., Allen, D. R., Siskind, D. E., Lambert, A., and Livesey, N. J.:  
934 Measurements of mesospheric water vapor from 1992 to 2021 at three stations from the Network for the  
935 Detection of Atmospheric Composition Change, *J. Geophys. Res. Atmos.*, 127(21), e2022JD037227,  
936 <https://doi.org/10.1029/2022JD037227>, 2022.

937 Perminov, V. I., Semenov, A. I., Pertsev, N. N., Medvedeva, I. V., Dalin, P. A., and Sukhodoiev, V. A.: Multi-  
938 year behavior of the midnight OH\* temperature according to observations at Zvenigorod over 2000-2016,  
939 *Adv. Space Res.*, 61, 1901-1908, <https://doi.org/10.1016/j.asr.2017.07020>, 2018.

940 Perminov, V. I., Pertsev, N. N., Dalin, P. A., Zheleznov, Yu. A., Sukhodolev, V. A., and Orekhov, M. D.:  
941 Seasonal and long-term changes in the intensity of O<sub>2</sub>(b<sup>1</sup>Σ) and OH(X<sup>2</sup>Π) airglow in the mesopause region,  
942 *Geomagn. Aeron.*, 61, 589-599, <https://doi.org/10.1134/S0016793221040113>, 2021.

943 Perrone, L., and Mikhailov, A. V.: Long-term variations of exospheric temperature inferred from foF1  
944 observations: A comparison to ISR Ti trend estimates. *J. Geophys. Res. Space Phys.*, 122, 8883-8892,  
945 <https://doi.org/10.1029/2017JA024193>, 2017.

946 Perrone, L., and Mikhailov, A. V.: Long-term variations of June column atomic oxygen abundance in the upper  
947 atmosphere inferred from ionospheric observations, *J. Geophys. Res. Space Phys.*, 124, 6305-6312,  
948 <https://doi.org/10.1029/2019JA026818>, 2019.



949 Qian, L., Jacobi, C., and McInerney, J.: Trends and solar irradiance effects in the mesosphere, *J. Geophys. Res.*  
950 *Space Phys.*, 124, 1343-1360, <https://doi.org/10.1029/2018JA026367>, 2019.

951 Qian, L., McInerney, J. M., Solomon, S. S., Liu, H., and Burns, A. G.: Climate changes in the upper atmosphere:  
952 Contributions by the changing greenhouse gas concentrations and Earth's magnetic field from the 1960s to  
953 2010s, *J. Geophys. Res. Space Phys.*, 126(3), e2020JA029067, <https://doi.org/10.1029/2020JA029067>,  
954 2021.

955 Ramesh, K., and Smith, A. K.: Long-term variability and tendencies in non-migrating diurnal tide from  
956 WACCM6 simulations during 1850-2014, *J. Geophys. Res. Space Phys.*, 126(3), e2020JA028904,  
957 <https://doi.org/10.1029/2020JA028904>, 2021.

958 Ramesh, K., Smith A. K., Garcia, R. R., Marsh, D. R., Sridharan, S., and Kishore Kumar, K.: Long-term  
959 variability and tendencies in migrating diurnal tide from WACCM6 simulations during 1850-2014, *J.*  
960 *Geophys. Res. Atmos.*, 125(23), e2020JD033644, <https://doi.org/10.1029/2020JD033644>, 2020a.

961 Ramesh, K., Smith A. K., Garcia, R. R., Marsh, D. R., Sridharan, S., and Kishore Kumar, K.: Long-term  
962 variability and tendencies in the middle atmosphere temperature and zonal wind from WACCM6  
963 simulations during 1850-2014, *J. Geophys. Res. Atmos.*, 125(24), e2020JD033579,  
964 <https://doi.org/10.1029/2020JD033579>, 2020b.

965 Rezac, L., Yue, J., Yongxiao, J., Russell, J. M., III, Garcia, R., López-Puertas, M., and Mlynarczyk, M. G.: On  
966 long-term SABER CO<sub>2</sub> trends and effects due to non-uniform space and time sampling, *J. Geophys. Res.*  
967 *Space Phys.*, 123, 7958–1967, <https://doi.org/10.1029/2018JA025892>, 2018.

968 Rishbeth, H.: A greenhouse effect in the ionosphere? *Planet. Space Sci.*, 38, 945–948, 1990.

969 Rishbeth, H., and Roble, R. G.: Cooling of the upper atmosphere by enhanced greenhouse gases - modelling of  
970 thermospheric and ionospheric effects. *Planet. Space Sci.*, 40, 1011-1026, 1992.

971 Roble, R. G., and Dickinson, R. E.: How will changes in carbon dioxide and methane modify the mean structure  
972 of the mesosphere and lower thermosphere? *Geophys. Res. Lett.*, 16, 1441–1444, 1989.

973 Sergeenko, N. P.: Long-term dynamics of the properties of ionospheric F2-layer disturbances in various regions.  
974 *Geomagn. Aeron.*, 61, 234-240, <https://10.1134/S0016793221020158>, 2021.

975 Sharan, A., and Kumar, S.: Long-term trends of the F2 region at mid-latitudes in the Southern Hemisphere, *J.*  
976 *Atmos. So.-Terr. Phys.*, 220, 105683, <https://doi.org/10.1016/j.jastp.2021.105683>, 2021.

977 She, C.-Y., Berger, U., Yan, Z.-A., Yuan, T., Lübken, F.-J., Krueger, D. A., and Hu, X.: Long-term trend of  
978 midlatitude mesopause region temperature based on 28 years (1990-2017) of Na lidar observations, *J.*  
979 *Geophys. Res. Space Phys.*, 124, 7140-7156, <https://doi.org/10.1029/2019JA026759>, 2019.

980 Solomon, S. C., Liu, H.-L., Marsh, D. R., McInerney, J. M., Qian, L., and Vitt, F. M.: Whole atmosphere climate  
981 change: Dependence on solar activity, *J. Geophys. Res. Space Phys.*, 124, 3799-3809,  
982 <https://doi.org/10.1029/2019JA026678>, 2019.

983 Venkat Ratnam, M., Akhil Raj, S.T., and Qian, L.: Long-term trends in the low-latitude middle atmosphere  
984 temperature and winds: Observations and WACCM-X model simulations, *J. Geophys. Res. Space Phys.*,  
985 124, 7320-7331, <https://doi.org/10.1029/2019JA026928>, 2019.

986 Vincent, R. A., Kovalam, S., Murphy, D. J., Reid, I. M., and Younger, J. P.: Trends and variability in vertical  
987 winds in the Southern Hemisphere summer polar mesosphere and lower thermosphere, *J. Geophys. Res.*  
988 *Atmos.*, 124, 11070-11085, <https://doi.org/10.1029/2019JD030735>, 2019.

989 Weng, L., Lei, J., Zhong, J., Dou, X., and Fang, H.: A machine-learning approach to derive long-term trends of  
990 thermospheric density, *Geophys. Res. Lett.*, 47(3), e2020GL087140,  
991 <https://doi.org/10.1029/2020GL087140>, 2020.

992 Wilhelm, S., Stober, G., and Brown, P.: Climatologies and long-term changes in mesospheric wind and wave  
993 measurements based on radar observations at high and mid latitudes, *Ann. Geophys.*, 37, 851-875,  
994 <https://doi.org/10.5194/angeo-37-851-2019>, 2019.

995 Yu, W., Garcia, R., Yue, J., Russell, J. III, and Mlynczak, M.: Variability of water vapor in the tropical middle  
996 atmosphere observed from satellites and interpreted using SD-WACCM simulations, *J. Geophys. Res.*  
997 *Atmos.*, 127(13), e2022JD036714, <https://doi.org/10.1029/2022JD036714>, 2022.

998 Yuan, T., Solomon, S. C., She, C.-Y., Krueger, D. A., and Liu, H.-L.: The long-term trends of nocturnal  
999 mesopause temperature and altitude revealed by Na lidar observations between 1990 and 2018 at  
1000 midlatitude, *J. Geophys. Res. Atmos.*, 124, 5970-5980, <https://doi.org/10.1029/2018JD029828>, 2019.

1001 Yue, J., Russell, J. III, Gan, Q., Wang, T., Rong, P., Garcia, R., and Mlynczak, M.: Increasing water vapor in the  
1002 stratosphere and mesosphere after 2002, *Geophys. Res. Lett.*, 46, 13452-13460,  
1003 <https://doi.org/10.1029/2019GL084973>, 2019.

1004 Yue, X., Hu, L., Wei, Y., Wan, W., and Ning, B.: Ionospheric trend over Wuhan during 1947-2017: Comparison  
1005 between simulation and observation, *J. Geophys. Res. Space Phys.*, 123, 1396-1409,  
1006 <https://doi.org/10.1002/2017JA024675>, 2018.

1007 Yue, X., Cai, Y., Ren, Z., Zhou, X., Wei, Y., and Pan, Y.: Simulated long-term evolution of the ionosphere  
1008 during Holocene, *J. Geophys. Res. Space Phys.*, 127(11), e2022JA031042,  
1009 <https://doi.org/10.1029/2022JA031042>, 2022.

1010 Zhang, S.-R., Holt, J. M., Erickson, P. J., and Goncharenko, L. P.: Comments on “Long-term variations of  
1011 exospheric temperatures inferred from foF1 observations: A comparison to ISR Ti trend estimates” by  
1012 Perrone and Mikhailov, *J. Geophys. Res. Space Phys.*, 123, 4467-4473,  
1013 <https://doi.org/10.1029/2017JA024948>, 2018.

1014 Zhao, X. R., Sheng, Z., Shi, H. Q., Weng, L. B., and Liao, Q. X.: Long-term trends and solar responses of the  
1015 mesopause temperatures observed by SABER during the 2002-2019 period, *J. Geophys. Res. Atmos.*,  
1016 125(11), e2020JD032418, <https://doi.org/10.1029/2020JD032418>, 2020.

1017 Zhao, X. R., Sheng, Z., Shi, H. Q., Weng, L. B., and He, Y.: Middle atmosphere temperature changes derive  
1018 from SABER observations during 2002-2020, *J. Clim.*, 34, 7995-8012, <https://doi.org/10.1175/JCLI-D-20-1010.1>, 2021.

1019

1020 Zhou, X., Yue, X., Ren, Z., Liu, Y., Cai, Y., Ding, F., and Wei, Y.: Impact of anthropogenic emission changes  
1021 on the occurrence of equatorial plasma bubbles, *Geophys. Res. Lett.*, 49(3), e2021GL097354,  
1022 <https://doi.org/10.1029/2021GL097354>, 2022.

1023

1024

1025

1026

1027 **Figure 1.** Yearly values of foF2 residuals after removing solar influence for Pruhonice, 1996-2014. Green curve - solar  
1028 activity proxy F10.7; blue curve – solar proxy F30; red curve – solar proxy Mg II; longer-dash colored lines – respective

1029 linear trends; short-dash black horizontal line – zero difference level. A negative difference means smaller observed than  
1030 model value. After Laštovička (2021b).

1031  
1032 **Figure 2.** Temperature trends (K per decade) vs. altitude from 20 to 100 km at 20° N (a) and 44° N (b). Black: trends based on  
1033 SABER zonal means over longitude and local time; blue: based on zonal means at 00:00 LT; green: 06:00 LT, red: 12:00 LT,  
1034 magenta: 18:00 LT. After Huang and Mayr (2021).

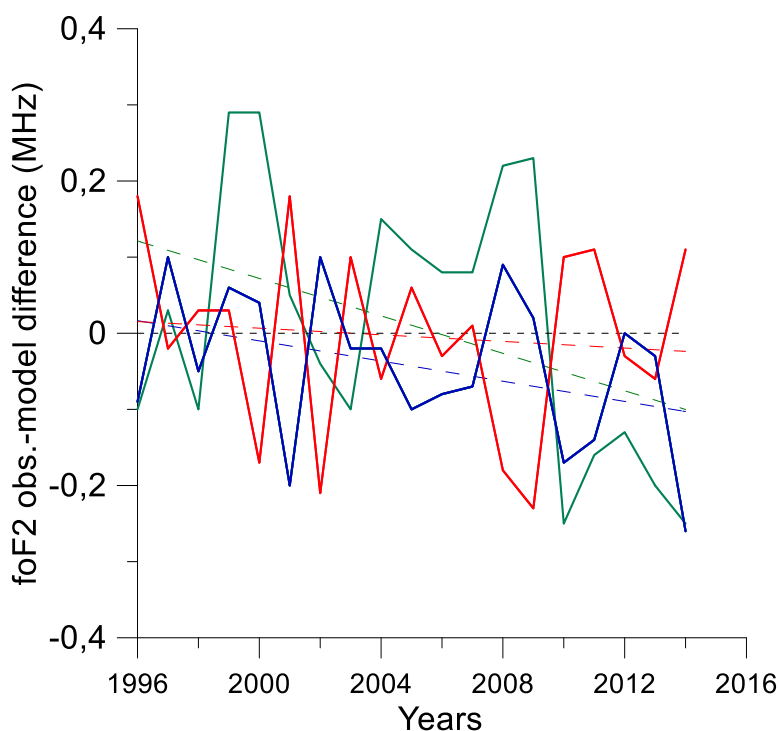
1035  
1036 **Figure 3.** Average monthly mean zonal wind at 0.001 hPa (~90 km) for March, June, September, and December, simulated  
1037 by model WACCM-X for the period of 2000–2014 (top row). The corresponding zonal wind trends (middle row). The  
1038 corresponding solar irradiance effect on the zonal winds (lower row). After Qian et al. (2019).

1039  
1040 **Figure 4.** Seasonal variations of the trend slope/coefficient of foE for various LT moments for Juliusruh station (54.6°N,  
1041 13.4°E). After Danilov and Konstantinova (2019).

1042  
1043 **Figure 5.** Left panels show the global distributions of neutral temperature  $T_n$  at 300 km, ion temperature  $T_i$  at 300 km,  
1044 electron temperature  $T_e$  at 400 km and neutral density  $\rho$  at 400 km in the 1960s. Right panels show changes of global  
1045 distributions of these four parameters from the 1960s to the 2010s separately for the effect of greenhouse gases (GHGs, in the  
1046 thermosphere essentially  $\text{CO}_2$ , left part) and of the secular change of the Earth's magnetic field (right part). After Qian et al.  
1047 (2021).

1048  
1049

1050  
1051



1052  
1053  
1054  
1055  
1056  
1057  
1058  
1059  
1060  
1061  
1062  
1063  
1064  
1065  
1066  
1067  
1068  
1069  
1070  
1071  
1072  
1073  
1074  
1075  
1076

Fig. 1

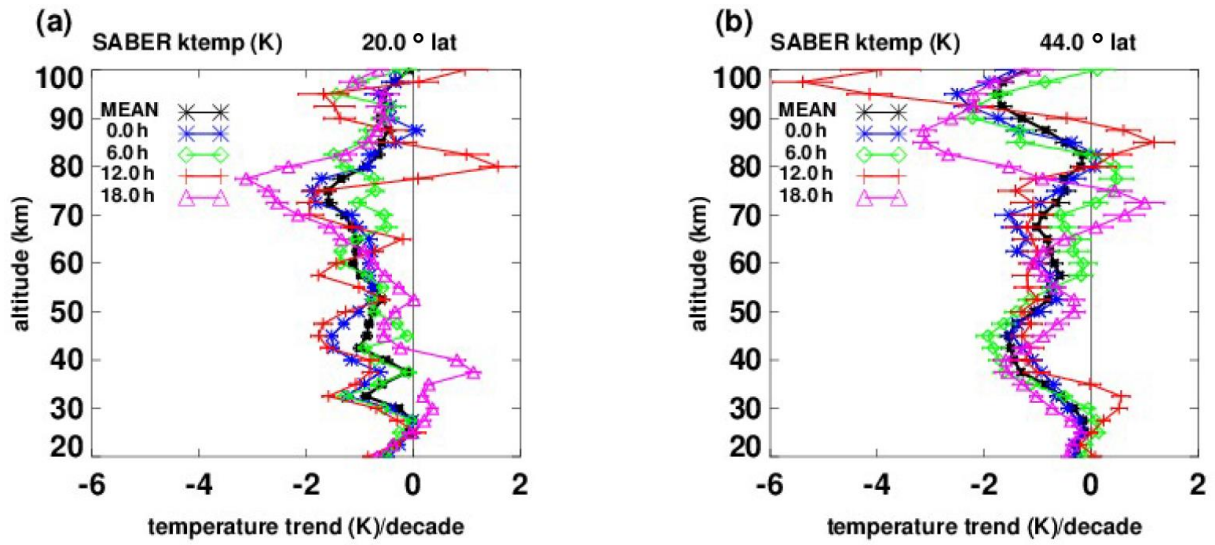


Fig. 2

1077  
1078  
1079  
1080  
1081  
1082

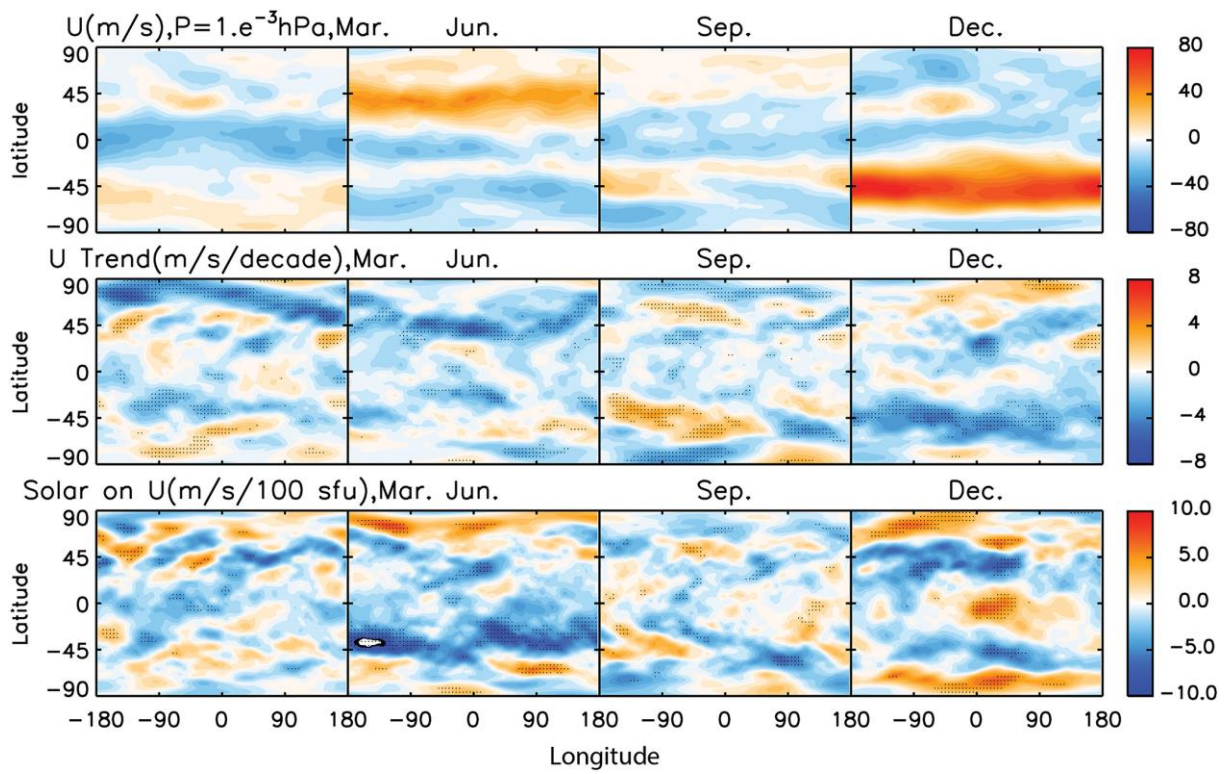


Fig.3

1083  
1084  
1085  
1086  
1087  
1088  
1089

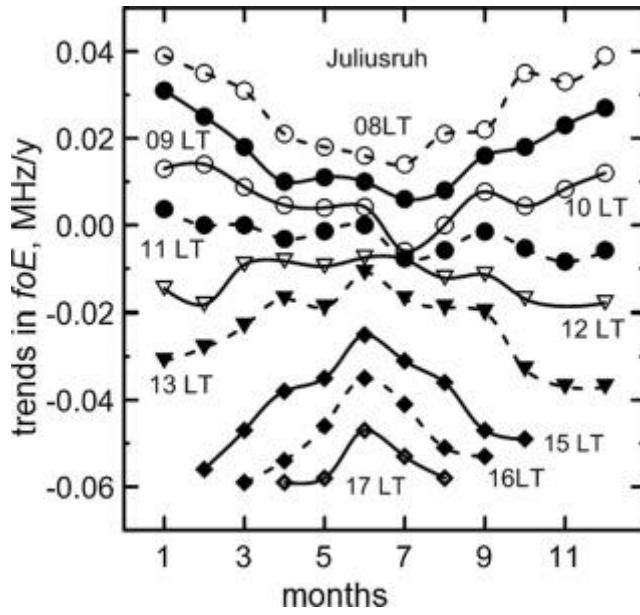


Fig. 4

1090  
1091  
1092  
1093  
1094  
1095  
1096

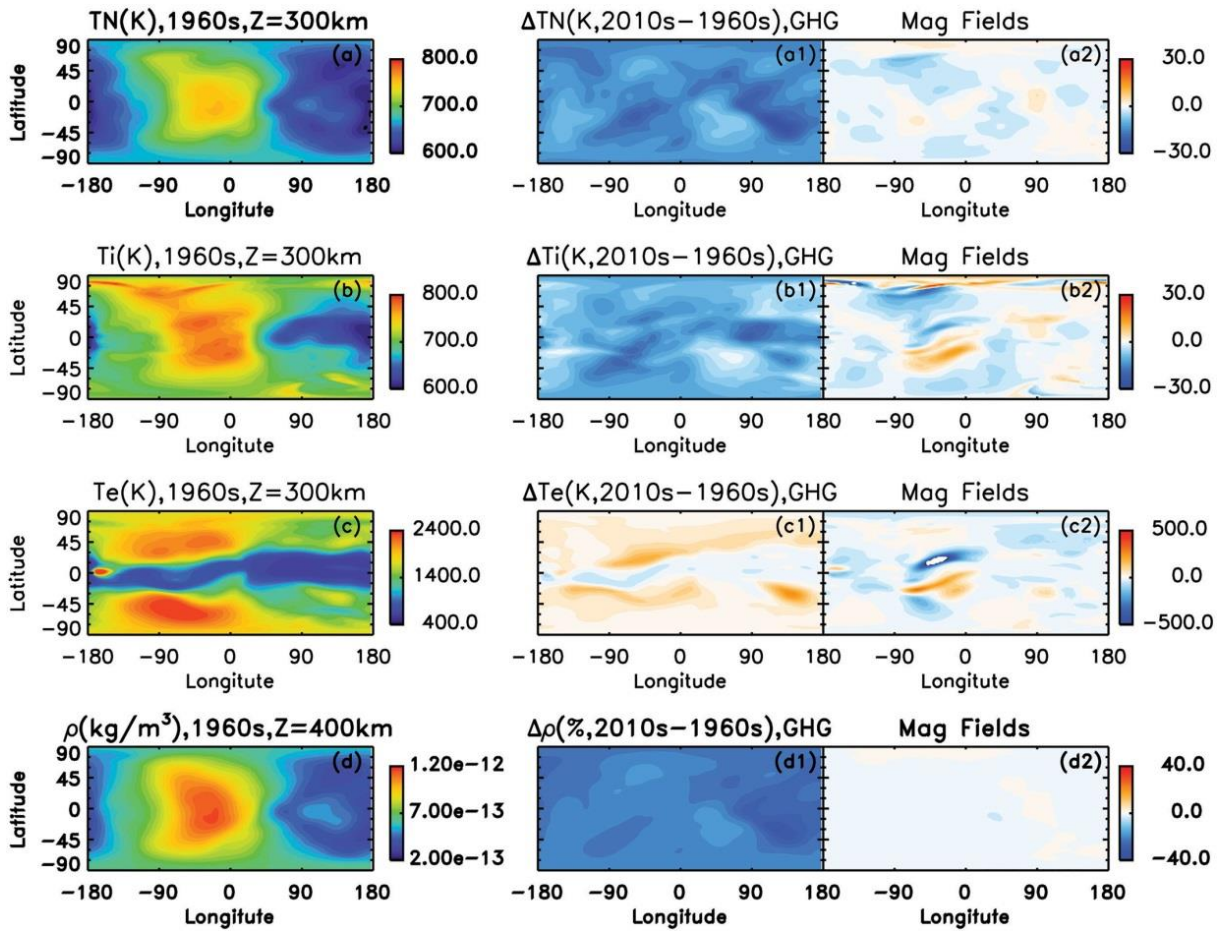


Fig. 5

1097  
1098  
1099